Transverse vibration of a beam excited axially by an harmonic motion transmitted through intermittent contact

Daniel Cintra, Gwendal Cumunel, Pierre Argoul

Transverse vibration of a beam excited axially by an harmonic motion transmitted through permanent or intermittent elastic contact

Daniel Cintra (corresponding author), Gwendal Cumunel
Université Paris-Est,
Laboratoire Navier (UMR 8205), CNRS, ENPC, IFSTTAR,
6 et 8, avenue Blaise Pascal,
Cité Descartes, Champs-sur-Marne,
F-77455 Marne La Vallée Cedex 2, France.
email: daniel.cintra@enpc.fr, gwendal.cumunel@enpc.fr
and
Pierre Argoul
IFSTTAR, Laboratoire MAST-SDOA,
F-77455 Marne La Vallée, Cedex 2, France
email: pierre.argoul@ifsttar.fr

Abstract

The transverse vibration of a beam excited axially by an harmonic motion transmitted through intermittent or permanent elastic contact is studied. It is shown that this vibration is governed by a non-linear argumental equation, which means that a vibration in the fundamental transverse mode of the beam can occur when the frequency of the excitation is many times the frequency of the fundamental transverse mode. Two cases are considered : the hinged-(hinged-guided) case, and the clamped-(clamped-guided) case. A "natural" model is given. An approached smoothed model is derived. The averaging method gives a standard system of differential equations for the smoothed model. Symbolic relations are derived for the smoothed model. Numeric simulations allow a comparison between the natural model and the smoothed model. They also constitute a guide to the choice of parameters for the natural model. Experimental results are given and compared to the natural and the smoothed models.

Keywords— non-linear; argumental oscillator; beam; axial excitation; transverse; spatial modulation; Van der Pol representation.

Contents

1 Introduction.

The so-called argumental oscillator was discovered by Béthenod [1] in 1938, although the word "argumental" was forged by Russian physicists in 1973 [11] who studied the phenomenon. Further developments were carried out by Doubochinski [8, 9], particularly the discovery of the multiple resonance and the quantum effect. The argumental oscillator has a stable motion consisting of a periodic motion at a frequency next to its natural frequency when submitted to an external force whose frequency is close to a multiple of said natural frequency. One condition for the phenomenon to arise is that the external force be dependent on the space coordinate of the oscillator. Argumental oscillations have also been observed and described in [7,12]. They have also been studied in [3–6].

The typical second-order ordinary differential equation for a one-degree-of-freedom argumental oscillator is:

$$\ddot{x} + 2\beta\omega_0\dot{x} + \omega_0^2 x = g_1(x) + g_2(x)cos(\nu t) \tag{1}$$

In this paper, a beam submitted to an axial harmonic excitation is studied. The beam "senses" the excitation when it is near its resting position, and does not sense it any more when it is in a sufficiently bended position. This is realized by way of an intermittent contact. This configuration should allow to study the behaviour of a structure when two elements are close to each other, but disconnected, be it by design or after damaging.

2 System configuration.

The schematic system configuration is as shown in Fig. 1. A beam is represented, with its left end S and right end M, in an hinged-(hinged-guided) configuration. Point M is intermittently pushed to the left by a plate C, which is linked to a point A via a spring. $\vec{F}$ is the force intermittently applied by plate C to the beam's right end in M. Point A is in harmonic motion horizontally in the figure, in such a manner that the contact between plate C and point M be intermittent when the beam is in resting position, and a force F_0 is applied to point M when the beam is in resting position and point A is in center position.

3 Modelling.

In this section, a first model will be studied, called "natural model", because it is deduced directly from simple physical laws and the arrangement of the components beam, spring, and points M and A. This model involves a C^0-class function for the external force. This leads to a discontinuous model, involving a C^0-class function for the external force, due to the intermittent nature of the contact at point M.

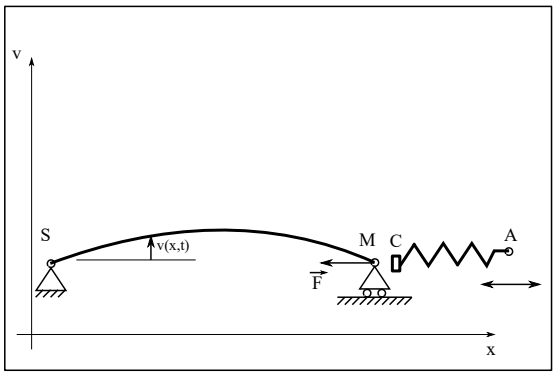

Figure 1: system configuration. x is the horizontal abscissa, v is the transverse displacement, t is the time, and $\vec{F}$ is the force applied by plate C to point M.

Then a second model will be studied, called a "smoothed model", because it is an approximation to the natural model. This model is not as close to physical reality as the natural model, but, in exchange, involves a C^∞-class function for the external force, easier to manipulate.

3.1 Expression of point M's abscissa x_M.

We shall need this expression to calculate the force F. As the beam bends, point M moves to the left. Define L = beam's length and x_M = point M's abscissa. On the beam, define the curvilinear abscissa from point S to current point (x, v) as $s(x, v, t)$. A classical method to calculate x_M is as follows.
As the beam is considered inextensible, point M's curvilinear abscissa is always equal to L, i.e.

$$s(x_M, v, t) = L = \int_0^{x_M} \sqrt{1 + \left(\frac{\partial v(u,t)}{\partial u}\right)^2}\, du \tag{2}$$

Then, using the limited development $\sqrt{1 + \left(\frac{\partial v(u,t)}{\partial u}\right)^2} \approx 1 + \frac{1}{2}\left(\frac{\partial v(u,t)}{\partial u}\right)^2$ inside Equ. (2), and considering that $\int_0^{x_M} \left(\frac{\partial v(u,t)}{\partial u}\right)^2 du \approx \int_0^{L} \left(\frac{\partial v(u,t)}{\partial u}\right)^2 du$, one gets:

$$x_M \approx L - \frac{1}{2}\int_0^{L} \left(\frac{\partial v(u,t)}{\partial u}\right)^2 du \tag{3}$$

Then, consider that transverse motion is expressed as

$$v(x,t) = L q_1(t) \varphi(x), \tag{4}$$

where $\varphi(x)$ is the modal form of the first mode and $q_1(t)$ is the amplitude as a function of time.

Hinged-(hinged-guided) case. In this case, consider that the first mode is $\varphi(x) = \sin\left(\pi\dfrac{x}{L}\right)$. Substituting this expression into Equ. (4), then $v(x,t)$ into (3), one gets:

$$x_M(t) \approx L\left(1 - \frac{\pi^2}{4}q_1^2(t)\right)$$

Clamped-(clamped-guided) case. In this case, consider that the modal form of the first mode is (see [Pecker, chap.8, p.169]):

$$\varphi(x) = A_1\left[\sin(ax) - 1.0178\cos(ax) - \sinh(ax) + 1.0178\cosh(ax)\right]$$

with A_1 arbitrary.
Approach this modal form with

$$\varphi(x) = \frac{1}{2}\left(1 - \cos\left(\frac{2\pi x}{L}\right)\right), \tag{5}$$

It can be seen in Fig. 2 that, if $A_1 = 0.6024$, the approaching curve is close to the original curve. Hence, substituting (5) into (4), and then $v(x,t)$ into (3)

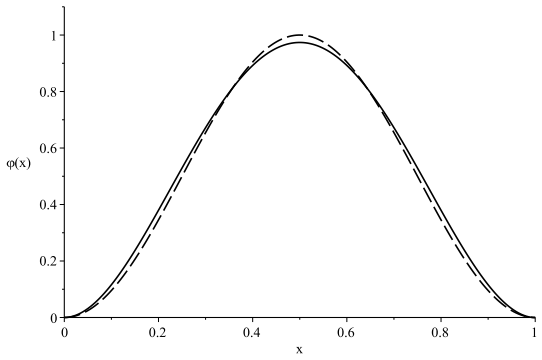

Figure 2: Approached modal form: exact (solid line), approached (dotted line).

yields:

$$x_M(t) = L\left(1 - \frac{\pi^2}{4}q_1^2(t)\right)$$

Conclusion about both cases. Consequently, one can put:

$$x_M(t) = L\left(1 - \frac{\pi^2}{4}q_1^2(t)\right) \tag{6}$$

for both the hinged-(hinged-guided) case and the clamped-(clamped-guided) case.

3.2 Natural model of force F.

Define x_A =point A's abscissa, $x_{A0} = \overline{x_A}$, where the overline notation means the averaging operation versus time. Define

$$z_A(t) = \frac{x_A(t) - x_{A0}}{L}. \tag{7}$$

It is easily seen that, provided there is contact between C and M,

$$F = F_0 + kL\left(z_A(t) + \frac{\pi^2}{4}q_1^2(t)\right)$$

where F is the expression of force, k is the spring's stiffness, z_A is given by equation (7) and x_M is given by Equ. (6).
Define $F_C(q_1,t) = F_0 + kL\left(z_A(t) + \frac{\pi^2}{4}q_1^2(t)\right)$. If the contact is intermittent, one has:

$$\begin{cases} F(q_1,t) = F_C(q_1,t) & if\ F_C(q_1,t) \le 0 \\ F(q_1,t) = 0 & otherwise \end{cases}$$

Define a_A as the amplitude of A's harmonic motion, normalized by L, i.e. $x_A(t) = x_{A0} + L\,a_A\cos(\nu t)$. Then $z_A(t) = a_A\cos(\nu t)$, and

$$\begin{cases} F(q_1,t) = F_0 + kL\left(a_A\cos(\nu t) + \frac{\pi^2}{4}q_1^2(t)\right) & if\ F_0 + kL\left(a_A\cos(\nu t) + \frac{\pi^2}{4}q_1^2(t)\right) \le 0 \\ F(q_1,t) = 0 & otherwise \end{cases} \tag{8}$$

3.3 Smoothed model of force F.

In this section, a truncated sinusoid is approximated by a sinusoid of same frequency and of lower amplitude, whose extremums are adjusted in reference to the truncated sinusoid. This leads to a continuous model.

3.3.1 High line and Low line.

An approaching function F_{approx} for $F(x,t)$ will be defined below. As k is generally a high value, define, for the sake of clarity, y_{approx} and y_{exact} by $y_{approx}(x,t) = F_{approx}(x,t)/(kL)$ and $y_{exact}(x,t) = F(x,t)/(kL)$.
The case where $F_0/(kL) < 0$ when $x = 0$ will be studied. That is, when the external excitation is off and the beam is at rest, there is contact between points M and C. In Figs. 3 to 6, various plots of the beam's transverse motion are represented. The values of the parameters are as follows: $F_0/(kL) = -2\ 10^{-3}$, $a_A = 1.8\ 10^{-3}$.
The case represented is when $\frac{F_0}{kL} + a_A < 0$, i.e. when the beam is at rest and the excitation is on, the contact between points M and C is never disrupted.

This can be seen in Fig. 3.
The plot of y_{exact} is a truncated sinusoid represented in the Figs. 3 to 6 by a solid line, along with the plot of y_{approx} in dashed line, and dotted construction lines showing the entirety of the truncated sinusoid, as well of various indications.
As soon as the sinusoid crosses the line $y = 0$, it gets truncated, and the only remaining part is located below said line.
From Equ. (8), it can be seen that the dotted horizontal marker line labelled $F_0/(kL) + a_A + \pi^2 x^2/4$ locates the top of the untruncated sinusoid, while the marker line labelled $F_0/(kL) - a_A + \pi^2 x^2/4$ locates the bottom of said sinusoid. The dotted horizontal markers labelled "High line" and "Low line" locate the highest (resp. lowest) point of the remaining part of the sinusoid after truncation.
Knowing that the excitation frequency is significantly greater than the beam's frequency (at least four times greater), consider that during one period of the excitation, the value of x is approximately constant, and the force F can be represented as a pure sinusoid, possibly truncated. It can be seen that the more x increases, the more the plot of y_{exact} (solid line) moves to the top of the figure, and the less the remaining part of the sinusoid is significant.
Denoting by Hl and Ll the High line's and Low line's ordinates, it holds:

$$\begin{cases} Hl(x) = \dfrac{F_0}{kL} + a_A + \dfrac{\pi^2 x^2}{4} & if\ \dfrac{F_0}{kL} + a_A + \dfrac{\pi^2 x^2}{4} \leq 0 \\ Hl(x) = 0 & otherwise \end{cases}$$

and

$$\begin{cases} Ll(x) = \dfrac{F_0}{kL} - a_A + \dfrac{\pi^2 x^2}{4} & if\ \dfrac{F_0}{kL} - a_A + \dfrac{\pi^2 x^2}{4} \leq 0 \\ Ll(x) = 0 & otherwise \end{cases}$$

The method employed in this section consists in approximating the exact function y_{exact} by a full sinusoid y_{approx} located between the High line and the Low line. It holds:

$$y_{approx}(t) = \frac{High\ line + Low\ line}{2} + \frac{High\ line - Low\ line}{2}\cos(\nu t) \quad (9)$$

$$= Mean(y_{approx}) + Ampl(y_{approx})\cos(\nu t) \quad (10)$$

where $Mean(f)$ denotes the mean value of function f over one period of f and $Ampl(f)$ denotes the amplitude of function f, i.e. half the difference between the maximum and minimum values of $f(t)$ over one period of f.

3.3.2 Approximation to a C^0-function.

An approximation to following function J will be needed hereinafter. Define function $J(x)$ as follows:

$$\begin{cases} J(x) = \alpha + \beta x^2 & if\ \alpha + \beta x^2 \leq 0 \\ J(x) = 0 & otherwise \end{cases}$$

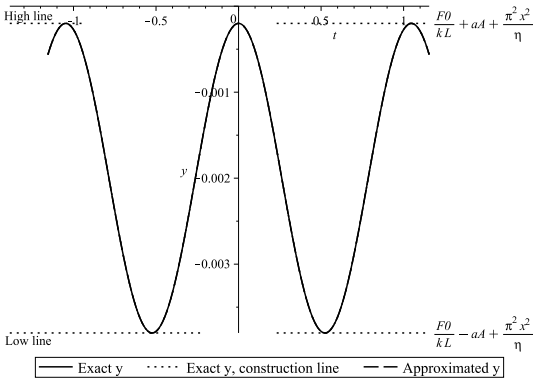

Figure 3: Exact and approached F, $x_{ref} = 0.0$, $a_A = -0.9\dfrac{F_0}{kL}$.

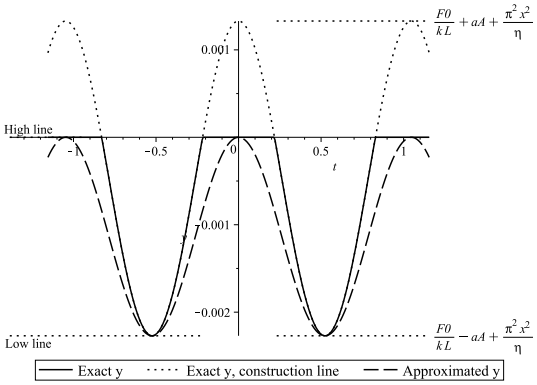

Figure 4: Exact and approached F, $x_{ref} = 0.015$, $a_A = -0.9\dfrac{F_0}{kL}$.

with $\alpha < 0$ and $\beta > 0$. This is a class C^0-function. Consider (see Fig. 7) that function $J_{approx} = \dfrac{\alpha}{1 + \lambda\frac{\beta}{\alpha}x^2}$, with $-8 \leq \lambda \leq -2$, is a fair approximation to $J(x)$. J_{approx} is of class C^∞.

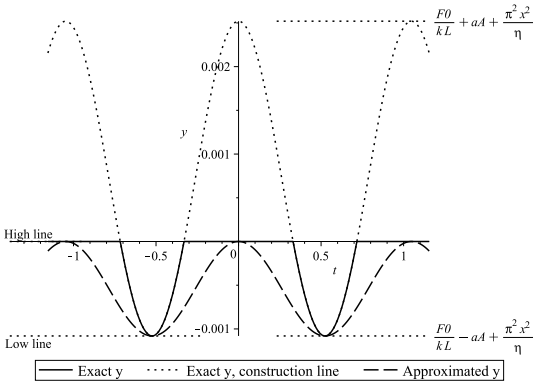

Figure 5: Exact and approached F, $x_{ref} = 0.02$, $a_A = -0.9\dfrac{F_0}{kL}$.

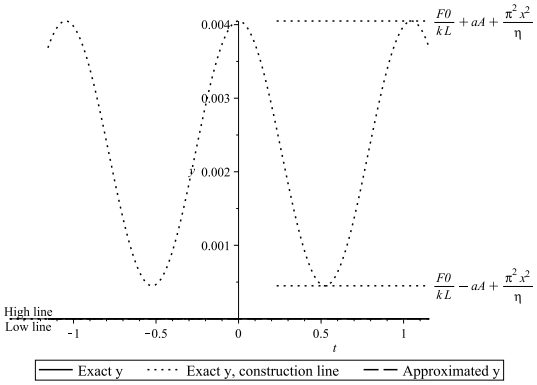

Figure 6: Exact and approached F, $x_{ref} = 0.025$, $a_A = -0.9\dfrac{F_0}{kL}$.

3.3.3 Approximation to the $Ampl(y_{approx})$ function.

Define $a_{Acrit} = \left|\dfrac{F_0}{kL}\right| = -\dfrac{F_0}{kL}$.
Form the expression of $Ampl(y_{approx}) = (Hl - Ll)/2$:

$$\begin{cases} Ampl(y_{approx}) & = a_A \qquad if\ \dfrac{\pi^2}{4}x^2 \leq a_{Acrit} - a_A \\ Ampl(y_{approx}) & = -\dfrac{1}{2}\left(\dfrac{F_0}{kL} - a_A + \dfrac{\pi^2}{4}x^2\right) \qquad if\ a_{Acrit} - a_A < \dfrac{\pi^2}{4}x^2 \leq a_{Acrit} + a_A \\ Ampl(y_{approx}) & = 0 \qquad if\ a_{Acrit} + a_A < \dfrac{\pi^2}{4}x^2 \end{cases}$$

which can be approximated by:

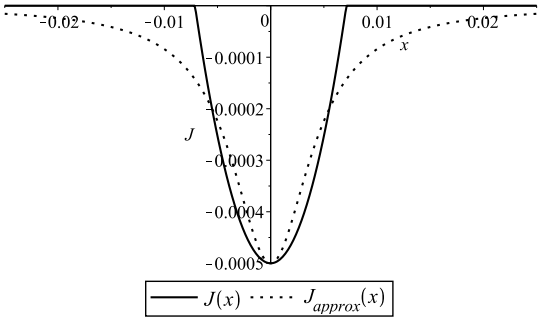

Figure 7: Exact and approached J, $\frac{F_0}{kL} = -0.1\ 10^{-2}$, $a_A = 0.05\ 10^{-2}$.

- if $a_A < a_{Acrit}$:

$$Ampl(y_{approx}) \approx \frac{a_A}{1 + Bx^2} \tag{11}$$

- otherwise:

$$Ampl(y_{approx}) \approx \frac{1}{2}\ \frac{-\frac{F_0}{kL} + a_A}{1 + Bx^2} \tag{12}$$

with $B = -\dfrac{\pi^2 kL}{4F_0}$.

3.3.4 Approximation to the $Mean(y_{approx})$ function.

Form the expression of $Mean(y_{approx}) = (Hl + Ll)/2$:

$$\begin{cases} Mean(y_{approx}) & = \dfrac{F_0}{kL} + \dfrac{\pi^2}{4}x^2 \qquad if\ \dfrac{\pi^2}{4}x^2 \leq a_{Acrit} - a_A \\ Mean(y_{approx}) & = \dfrac{1}{2}\left(\dfrac{F_0}{kL} - a_A + \dfrac{\pi^2}{4}x^2\right) \qquad if\ a_{Acrit} - a_A < \dfrac{\pi^2}{4}x^2 \leq a_{Acrit} + a_A \\ Mean(y_{approx}) & = 0 \qquad if\ a_{Acrit} + a_A < \dfrac{\pi^2}{4}x^2 \end{cases}$$

which can be approximated by:

- if $a_A < a_{Acrit}$:

$$Mean(y_{approx}) \approx \frac{F_0}{kL}\ \frac{1}{1 + Cx^2} \tag{13}$$

- otherwise:

$$Mean(y_{approx}) \approx \frac{1}{2}\ \frac{\frac{F_0}{kL} - a_A}{1 + Cx^2} \tag{14}$$

with $C = -\dfrac{\pi^2 kL}{2F_0}$.

3.3.5 Approximation to the F function.

Substituting Equations (11), (12), (13) and (14) into Equ. (10), and substituting F_{approx} for kLy_{approx}, one gets:

- if $a_A < a_{Acrit}$:

$$F_{approx} = F_0 \left(1 - \frac{Cx^2}{1+Cx^2}\right) + \frac{kLa_A}{1+Bx^2}\cos(\nu t) \tag{15}$$

- otherwise:

$$F_{approx} = \frac{1}{2}(F_0 - kL\, a_A)\left(1 - \frac{Cx^2}{1+Cx^2}\right) - \frac{1}{2}\frac{F_0 - kL\, a_A}{1+Bx^2}\cos(\nu t) \tag{16}$$

with $C = 2B = -\dfrac{\pi^2 kL}{2F_0}$.

4 Second-order differential equation of motion.

Equ. (6) gives x_M as a function of q_1, while Equations (15) and (16) give an approximated expression of the external force as a function of x and t. Substituting these expressions into the general equation to the modal coordinates, it is possible to obtain a second-order ordinary differential equation in $x(t)$.

4.1 Classical transverse motion of an axially-excited beam.

The classical equation of motion of an axially-excited Euler-Bernoulli beam is [10]:

$$\rho S\ddot{v} + EIv^{(4)} - F(\sigma,t)v'' + 2\beta'\dot{v} = f(x,t)$$

where S is the beam's cross-section area, E is the elastic modulus, I is the second moment of area of the beam's cross-section, F is the axial force, which may be a function of the beam's instantaneous state σ and of time t, $f(x,t)$ is the distributed load, β' represents the damping factor.
Using a change of variables $v(x,t) = Lq(t)\varphi(x)$, one obtains:

$$\rho S\ddot{q}(t)\varphi(x) + EI\varphi^{(4)}(x)q(t) - F(\sigma,t)\varphi''(x)q(t) + 2\beta'\varphi(x)\dot{q}(t) = f(x,t) \tag{17}$$

4.2 Projection onto the first mode.

Projecting Equ. (17) onto the first mode, one obtains, for the hinged-(hinged-guided) case:

$$\ddot{q}_1(t) + \frac{2\beta'}{\rho S}\dot{q}_1(t) + \left(\frac{\pi}{L}\right)^4 \frac{EI}{\rho S}q_1(t) + \left(\frac{\pi}{L}\right)^2 \frac{1}{\rho S}F(q_1,t)q_1(t) - \frac{4g}{\pi L} = 0 \tag{18}$$

with $v(x,t) \approx Lq_1(t)\sin\left(\frac{\pi}{L}x\right)$.
And for the clamped-(clamped-guided) case:

$$\ddot{q}_1(t) + \frac{2\beta'}{\rho S}\dot{q}_1(t) + \left(\frac{2\pi}{L}\right)^4 \frac{EI}{3\rho S}q_1(t) + \left(\frac{\pi}{L}\right)^2 \frac{1}{\rho S}F(q_1,t)q_1(t) - \frac{2g}{3L} = 0 \quad (19)$$

Introduce the beam's critical buckling force

$$F_B = \frac{\pi^2 EI}{a_3^2 L^2} \quad (20)$$

where L is the beam's length and a_3 is a coefficient equal to 1 in the hinged-(hinged-guided) case and 1/2 in the clamped-(clamped-guided) case.
Equations (18) and (19) can be rewritten into a unique expression:

$$\ddot{q}_1(t) + \frac{2\beta'}{\rho S}\dot{q}_1(t) + a_1\left(\frac{\pi}{L}\right)^2 \frac{F_B}{\rho S}q_1(t) + a_1\left(\frac{\pi}{L}\right)^2 \frac{1}{\rho S}F(q_1,t)q_1(t) - a_2\frac{g}{L} = 0 \quad (21)$$

with $a_1 = 1$, $a_2 = 4/\pi$ and $a_3 = 1$ in the hinged-(hinged-guided) case, and $a_1 = 4/3$, $a_2 = 2/3$ and $a_3 = 1/2$ in the clamped-(clamped-guided) case.

4.3 Second-order differential equation of motion with the natural model of the external force.

This equation will be of use below, to assess the quality of the approximated model which is given in section 3.
Substituting $F(q_1,t)$ as given in Equ. (8) into Equ. (21) while denoting $q_1(t)$ by y for the sake of clarity, one gets:

$$\ddot{y} + 2\beta\omega_0\dot{y} + \omega_0^2 y = -\omega_0^2 \frac{y}{F_B/(kL) + C_2/(kL)}F(y,t) + a_2\frac{g}{L} = 0 \quad (22)$$

with $\omega_0^2 = a_1\left(\frac{\pi}{L}\right)^2 \frac{F_B + C_2}{\rho S}$, $\beta\omega_0 = \frac{\beta'}{\rho S}$, and C_2=arbitrary constant.

4.4 Second-order differential equation of motion with the smoothed model of the external force.

Two cases must be distinguished, depending on the sign of $\frac{F_0}{kL} + a_A = a_A - a_{Acrit}$.
Denoting B for $B(a_A)$ and C for $C(a_A)$, and denoting y for q_1, one obtains, substituting F_{approx} as given in Equations (15) and (16) into Equ. (21):

- If $a_A < a_{Acrit}$:

$$\ddot{y} + 2\beta\omega_0\dot{y} + \omega_0^2 y = -\omega_1^2 \frac{By^3}{1+By^2} - a_2\frac{g}{L} + \omega_1^2 \frac{a_A}{\frac{F_0}{kL}} \frac{y}{1+Cy^2}\cos(\nu t)$$

- If $a_A \geq a_{Acrit}$:

$$\ddot{y} + 2\beta\omega_0\dot{y} + \omega_0^2 y = -\omega_2^2 \frac{By^3}{1+By^2} - a_2\frac{g}{L} - \omega_2^2 \frac{y}{1+By^2}\cos(\nu t) \qquad (23)$$

with

$$\omega_0^2 = a_1\left(\frac{\pi}{L}\right)^2 \frac{F_B+F_0}{\rho S},\ \omega_1^2 = -\frac{F_0}{F_B+F_0}\omega_0^2,$$
$$\omega_2^2 = -\frac{\frac{F_0-a_AkL}{2}}{F_B+\frac{F_0-a_AkL}{2}}\omega_0^2,\ C = 2B = -\frac{\pi^2 kL}{2F_0}.$$

Those equations are argumental equations similar to Equ. (1).

5 Applying the averaging method.

The averaging method [2] will be applied to the second-order differential equation of motion in y with the approximated form of the external force.

5.1 Reduced time.

Introducing the reduced time τ classically defined as $\tau = \omega_0 t$, and using from now on the dot notation to denote differentiation with respect to τ, one gets

$$\ddot{z} + 2\beta\dot{z} + z = -g(z) + AH(z)cos\left(\frac{\nu}{\omega_0}\tau\right)$$

with

- If $a_A < a_{Acrit}$:
  $A = \dfrac{1}{F_B+F_0}$ (denoted hereafter by A_1), $g(z) = -\dfrac{F_0}{F_B+F_0}\dfrac{Cz^3}{1+Cz^2} - \dfrac{a_2 g}{L\omega_0^2}$, and $H(z) = -kLa_A\dfrac{z}{1+Bz^2}$
- If $a_A \geq a_{Acrit}$:
  $A = \dfrac{2}{2F_B+F_0-a_AkL}$ (denoted hereafter by A_2), $g(z) = -\dfrac{F_0-a_AkL}{2F_B+F_0-a_AkL}\dfrac{Cz^3}{1+Cz^2} - \dfrac{a_2 g}{L\omega_0^2}$, and $H(z) = \dfrac{F_0-a_AkL}{2}\dfrac{z}{1+Bz^2}$

5.2 Standard system.

Searching a solution close to a slowly-varying sinusoid, carry out the following classic change of variables

$$\begin{cases} y(\tau) &= a(\tau)\sin(\rho\tau+\varphi(\tau)) \\ \dot{y}(\tau) &= a(\tau)\rho\cos(\rho\tau+\varphi(\tau)) \end{cases}$$

and obtain the standard system:

$$\begin{cases} \dot{a} &= \dfrac{\cos(\theta)}{\rho}\left(-2\beta\rho a\cos(\theta) - g(a\sin(\theta)) + AH(a\sin(\theta))E(\tau) + a\sin(\theta)(\rho^2-1)\right) \\ \dot{\varphi} &= -\dfrac{\sin(\theta)}{\rho a}\left(-2\beta\rho a\cos(\theta) - g(a\sin(\theta)) + AH(a\sin(\theta))E(\tau) + a\sin(\theta)(\rho^2-1)\right) \end{cases}$$

with $\theta = \rho\tau + \varphi$, $\rho = \dfrac{\omega}{\omega_0}$, ω= constant to be determined (close to 1), and $E(\tau) = \cos\left(\dfrac{\nu}{\omega_0}\tau\right)$.
The reciprocal relations are as follows, knowing that $a(\tau)$ is always positive:

$$\begin{cases} a(\tau) &= \sqrt{y^2(\tau) + \left(\dfrac{\dot{y}(\tau)}{\rho}\right)^2} \\ \varphi(\tau) &= \arctan\left(\rho\dfrac{y(\tau)}{\dot{y}(\tau)}\right) - \rho\tau \ [2\pi] \end{cases} \tag{24}$$

5.3 Averaged system.

Averaged expression of function g. Putting $G(a) = \overline{\sin(\theta)g(a\sin(\theta))}$, where the overline notation denotes averaging with respect to time over one period of the solution, one gets:

- If $a_A < a_{Acrit}$:

$$G(a) = -\frac{A_1}{2}F_0 a\left(1 - \frac{2}{Ca^2} + \frac{1}{Ca^2}\frac{2}{\sqrt{1+Ca^2}}\right) \tag{25}$$

- If $a_A \geq a_{Acrit}$:

$$G(a) = -\frac{A_2}{2}\frac{F_0 - a_A kL}{2}a\left(1 - \frac{2}{Ca^2} + \frac{1}{Ca^2}\frac{2}{\sqrt{1+Ca^2}}\right) \tag{26}$$

Decomposition of function $H(a\sin(\theta))$ in Fourier series of variable θ. $H(a\sin(\theta))$ being an odd function of variable θ, and being of period π, define its Fourier series coefficients h_q by

$$H(a\sin(\theta)) = \sum_{q=1,\ q\ odd}^{+\infty} h_q \sin(q\theta)$$

Then a calculus gives:

- If $a_A < a_{Acrit}$:
  $h_q = -a_A kL\dfrac{2}{B^{\frac{q+1}{2}}}\dfrac{(\sqrt{1+Ba^2}-1)^q}{\sqrt{1+Ba^2}a^q}$

- If $a_A \geq a_{Acrit}$:
  $h_q = \dfrac{F_0 - a_A kL}{2}\dfrac{2}{B^{\frac{q+1}{2}}}\dfrac{(\sqrt{1+Ba^2}-1)^q}{\sqrt{1+Ba^2}a^q}$

Calculus of $\overline{H(a\sin(\theta))}E(\tau)\cos(\theta)$. If $\dfrac{\nu}{\rho\omega_0}$ is an even integer (denoted by n), one gets $\overline{H(a\sin(\theta))E(\tau)\cos(\theta)} = \dfrac{1}{4}S_n\sin(n\varphi)$, with $S_n = h_{n-1} + h_{n+1}$. Otherwise, $\overline{H(a\sin(\theta))E(\tau)\cos(\theta)} = 0$.

Calculus of $\overline{H(a\sin(\theta))}E(\tau)\sin(\theta)$. If $\dfrac{\nu}{\rho\omega_0}$ is an even integer (denoted by n), one gets $\overline{H(a\sin(\theta))E(\tau)\sin(\theta)} = -\dfrac{1}{4}D_n\cos(n\varphi)$, with $D_n = h_{n-1} + h_{n+1}$. Otherwise, $\overline{H(a\sin(\theta))E(\tau)\sin(\theta)} = 0$.

Symbolic expressions of functions S_n and D_n . A calculus gives

$$\begin{aligned} S_n &= J\frac{4}{a^{n+1}}\frac{(\sqrt{1+Ba^2}-1)^n}{b^{\frac{n}{2}+1}} \\ D_n &= \frac{S_n}{\sqrt{1+Ba^2}} \end{aligned} \tag{27}$$

with $J = -a_A kL$ if $a_A < a_{Acrit}$, and $J = \dfrac{F_0 - a_A kL}{2}$ otherwise.
Also:

$$\begin{aligned} \frac{1}{S_n}\frac{\partial S_n}{\partial a} &= \frac{1}{a}\left(\frac{n}{\sqrt{1+Ba^2}} - 1\right) \\ \frac{1}{D_n}\frac{\partial D_n}{\partial a} &= \frac{1}{a}\left(\frac{n}{\sqrt{1+Ba^2}} - 2 + \frac{1}{1+Ba^2}\right) \end{aligned}$$

ρ against F_0. Recall that $\omega_0^2 = a_A\left(\dfrac{\pi}{L}\right)\dfrac{F_B + F_0}{\rho S}$. Put $\omega_{00} = \omega_0(F_0 = 0)$. Hence

$$\begin{cases} \omega_0 = \omega_{00}\sqrt{\dfrac{F_B + F_0}{F_B}} \\ \rho = \rho_{00}\sqrt{\dfrac{F_B}{F_B + F_0}} \\ \rho_{00} = \dfrac{\nu}{n\omega_{00}} \end{cases} \tag{28}$$

Because $F_0 \leq 0$, it holds $\rho \geq \rho_{00}$. And as it has been showed that $\rho > 1$ for any value of F_0 in the domain of this study, it consequently holds:

$$\rho_{00} \geq 1 \tag{29}$$

Averaged standard system. The classical averaging calculus gives, if $n = \dfrac{\nu}{\rho\omega_0}$ is an even integer:

$$\begin{cases} \dot{a} &= \dfrac{A}{4\rho n} S_n(a)\sin(n\varphi) - \beta a \\ \dot{\varphi} &= \dfrac{G(a)}{\rho a} + \dfrac{A}{4\rho a} D_n(a)\cos(n\varphi) - \dfrac{\rho^2-1}{2\rho} \end{cases} \tag{30}$$

If $n = \dfrac{\nu}{\rho\omega_0}$ is not an even integer, it holds:

$$\begin{cases} \dot{a} &= -\beta a \\ \dot{\varphi} &= \dfrac{G(a)}{\rho a} - \dfrac{\rho^2-1}{2\rho} \end{cases}$$

that is, the system behaves like if it were disconnected from the excitation source.

6 Stationary condition: properties expressed as symbolic expressions.

Making $\dot{a} = 0$ and $\dot{\varphi} = 0$ in system (30) constitutes the equations of the stationary condition:

$$\begin{cases} 0 &= \dfrac{A}{4\rho n} S_n(a_S)\sin(n\varphi_S) - \beta a_S \\ 0 &= G_1(a_S) + \dfrac{A}{4} D_n(a_S)\cos(n\varphi_S) - \dfrac{\rho^2-1}{2} \end{cases} \tag{31}$$

where a_S is the motion's amplitude and φ_S is the phase shift of said motion with respect to the excitation force, and function G_1 is defined as

$$G_1(a_S) = G(a_S)/a_S \tag{32}$$

From this system, one deduces a number of symbolic relations which give clues about the stationary condition.
Firstly, writing that $\sin^2(n\varphi_S) + \cos^2(n\varphi_S) = 1$, one gets:

$$(4\rho\beta)^2 + 4\frac{S_n^2(a_S)}{D_n^2(a_S)}\left(2G_1(a_S) - (\rho^2-1)\right)^2 = \frac{A^2 S_n^2(a_S)}{a_S^2} \tag{33}$$

Also, writing that $\tan(n\varphi_S) = \dfrac{\sin(n\varphi_S)}{\cos(n\varphi_S)}$, one gets:

$$\tan(n\varphi_S) = \frac{D_n(a_S)}{S_n(a_S)} \frac{2\rho\beta a_S}{a_S(\rho^2-1) - 2G(a_S)}$$

Fig. 8 shows the implicit curve giving a_A against a_S for the values of parameters

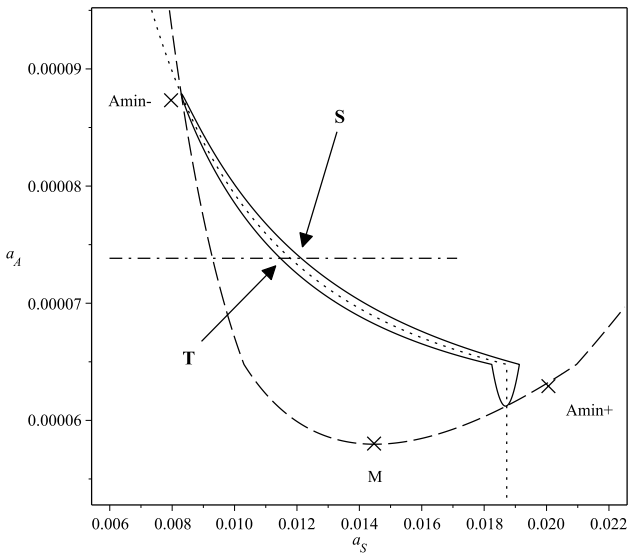

Figure 8: Stationary condition, averaged system with the smoothed model of the external force. a_S is the stationary-motion's amplitude, a_A is the excitation's amplitude. The dash-dotted line shows the value of a_A which will be used for the Van der Pol representation of Fig. 9. The dotted line is the G curve. The solid line is the solution of the averaged smooth model. The dashed line is the Beta curve. S and T respectively represent the stable and unstable stationary-motion points. A_{min-} and A_{min+} are the calculated points of intersection of the Beta-curve and the G-curve. M is the calculated minimum of the Beta-curve. Parameter values are: $n = 6$, $\beta = 2.4\ 10^{-3}$, $F_B = 51N$, $F_0 = -8N$, $L = 0.95m$, $k = 130\ kN/m$, $f_{00} = 6.615Hz$, $f_{shaker} = 39.500711Hz$, $\rho_{00} = 0.9952308$.

given in the figure's legend. The "Beta curve" represents the solution of the first equation of System (31) in which $n\varphi_S = -\pi/2$ is applied. The "G curve" represents the solution of:

$$2G_1(a_S) - (\rho^2 - 1) = 0 \tag{34}$$

The solid-line curve represents the solution of Equ. (33).
Points S, T, A_{min-}, A_{min+} and $M1$ are all calculated via symbolic formulas given below. Points A_{min-} and A_{min+} are the maximum and the minimum of the curve representing Equ. (33). Point M is the minimum of the Beta curve.
Observation of Fig. 8 shows that the solution of System (31) can be seen as composed of two arcs: one upper arc and one lower arc, in contact at their upper extremities close to point A_{min-} (on the left) and at their lower extremities via a V-shaped curve, near point A_{min+} (on the right). The upper (resp. lower) arc represents the stable (resp. unstable) stationary solutions. The left part of the V-shaped curve represents unstable stationary solutions, and the right

part stable ones. For a given value of the excitation, i.e. a given amplitude a_A, there are two possible values for a_S, represented by points S and T. Point S is the stable stationary condition, while point T is the unstable one. The V-shaped curve represents cases where there is permanent contact between the beam under test (BUT) and the excitation source when the BUt is in rectilinear position. In these cases, the contact may or may not stay permanent when the BUT enters a transversal vibration, depending on the amplitudes of transversal vibration of the BUT and of the excitation source. The arcs represent the other cases.

6.1 G-curve.

An interesting point is to search for a symbolic expression giving the coordinates of points A_{min-} and A_{min+}. Instead of searching for the exact values, which leads to intricate calculus, notice that these points are close to the intersection points of the Beta-curve and the G-curve. In this manner, calculus is simpler. As usual, two cases must be distinguished, depending on the sign of $a_A - a_{Acrit}$.

- If $a_A < a_{Acrit}$:
  Substituting the G and G_1 function definitions (25) and (32) into the G-curve's equation (34) yields:

$$R + 1 - \frac{2}{x} + \frac{1}{x}\frac{2}{\sqrt{x+1}} = 0 \tag{35}$$

  with

$$x = Ca_S^2 \tag{36}$$

  and $R = (\rho^2 - 1)\dfrac{F_B + F_0}{F_0}$.
  Moreover, due to relations (28), it holds:

$$R = \frac{(\rho_{00}^2 - 1)F_B - F_0}{F_0}$$

  so that $R < 0$, because of Equ. (29). Then, putting $u = \sqrt{x+1}$, one gets:

$$u^2 + u - \frac{2}{R+1} = 0 \tag{37}$$

  Then knowing that $Ca_S^2 > 0$, one concludes that a necessary condition for Equ. (37) to have real solutions is that

$$-1 < R < 0 \tag{38}$$

  and, therefore, that $(F_B + F_0)/F_B < \rho_{00} < 1$, which cannot be realized, because of (29). In conclusion, the G-curve cannot have any part of it inside the region $a_A < a_{Acrit}$. Therefore, from here on, only the case $a_A \geq a_{Acrit}$ will be considered.

- If $a_A \geq a_{Acrit}$:
  In the same manner as in the case $a_A < a_{Acrit}$, substituting the G and G_1 function definitions (26) and (32) into the G-curve's equation (34) yields formally the same Equ. (35) as hereabove, but with:

$$R = (\rho^2 - 1)\frac{2F_B + F_0 - a_A kL}{F_0 - a_A kL} \tag{39}$$

  One concludes that condition (38) is still necessary, with R depending here on a_A. Substituting (39) into (38) yields:

$$\frac{F_B + F_0}{F_B} < \rho_{00}^2 < \frac{F_B + F_0}{F_B + \frac{F_0 - a_A kL}{2}}$$

  The inequality on the left is always verified, because $F_0 < 0$ and $\rho_{00} > 1$. The inequality on the right is realizable, because it holds in this case: $a_A \geq a_{acrit}$, and therefore $F_0/(kL) + a_A \geq 0$.
  The G-curve's equation can be expressed as a_S^2 versus a_A:

$$x = \frac{2}{R(a_A) + 1} - \frac{1}{2} - \frac{1}{2}\sqrt{1 + \frac{8}{R(a_A) + 1}}$$

  with $x = Ca_S^2$.
  Then, an elementary calculus yields:

$$R(a_A) = \frac{2}{x}\left(1 - \frac{1}{\sqrt{x+1}}\right) - 1 \tag{40}$$

  From Equ. (36), (39) and (40), the reciprocal relation giving a_A against a_S can be calculated by classical ways. It holds:

$$a_A = \frac{F_0}{kL} + 2\frac{F_B}{kL}\frac{\rho^2 - 1}{\rho^2 - \frac{2}{Ca_S^2}\left(1 - \frac{1}{\sqrt{1 + Ca_S^2}}\right)} \tag{41}$$

  with ρ as given by relations (28).

6.2 Beta-curve.

Knowing that the G-curve cannot have any part of it inside the region $a_A < a_{Acrit}$, and that what is searched for is the intersection between the G-curve and the Beta-curve, consider only the case where $a_A \geq a_{Acrit}$ when studying the Beta-curve. The Beta-curve's equation is:

$$\frac{\rho\beta}{S_n(a_S)} = -\frac{A}{4a_S} \tag{42}$$

with a minus sign because here $S_n(a_S) < 0$ and $A = A_2 > 0$. Substitute the symbolic expression of S_n, as given by Equ. (27), into (42) to obtain the Beta-curve's equation:

$$-R(a_A)\frac{\rho\beta}{\rho^2-1} = \frac{1}{z}\left(\frac{\sqrt{1+z}-1}{\sqrt{z}}\right)^n \tag{43}$$

with

$$z = Ba_S^2 \tag{44}$$

and $R(a_A)$ given by (39).

6.3 Intersection of the Beta-curve and the G-curve.

This intersection consists of points A_{min-} and A_{min+}. Substituting the expression of R given by Equ. (40) into Equ. (43) and taking $C = 2B$ gives:

$$\frac{\rho\beta}{\rho^2-1}\left(1 + -\frac{1}{z} + \frac{1}{z\sqrt{2z+1}}\right) = \frac{1}{z}\left(\frac{\sqrt{1+z}-1}{\sqrt{z}}\right)^n \tag{45}$$

which is an equation in a_S^2 because of the definition of z in Equ. (44).

Limit condition for the existence of an intersection. There is a maximum value of $\frac{\rho\beta}{\rho^2-1}$ for Equ. (45) to have solutions. A good symbolic approximation of this limit value can be obtained by using Appendix A in Section 12 to find that

- $$\left(\frac{\rho\beta}{\rho^2-1}\right)_{max} \approx \frac{4n^2}{(n^2-4)^2}\left(\frac{n-2}{n+2}\right)^{n/2}; \tag{46}$$

- the abscissa in z of the tangency point is $z = z_{2max} = \frac{n^2}{4} - 1$. Hence, using Eqs.(**??**) and (44)), the corresponding value a_{Scrit} of a_S can be expressed:

$$a_{Scrit} = \sqrt{z_{2max}/B} = \frac{2n}{n^2-4}\left(\frac{n-2}{n+2}\right)^{n/4}\sqrt{-\frac{4F_0}{\pi^2 kL}}$$

- The ordinate a_{Acrit} of the tangency point is obtained by substituting the expression of a_S hereabove into Equ. (41), yielding

$$a_{Acrit} = \frac{F_0}{kL} + 2\frac{F_B}{kL}\frac{\rho^2-1}{\rho^2-N} \tag{47}$$

with $N = \frac{4}{n^2-4}\left(1 - \frac{1}{\sqrt{\frac{n^2}{2}-1}}\right)$.

Approximate symbolic solutions for the intersection. If the limit condition hereabove is satisfied, it is possible to solve approximately Equ. (45), using the following remarks:

- Function $1 - \frac{1}{z} + \frac{1}{z\sqrt{2z+1}}$ can be approximated by function $\frac{\sqrt{2}z}{1+\sqrt{2}z}$.
- Function $J(z) = \frac{1}{z}\left(\frac{\sqrt{1+z}-1}{\sqrt{z}}\right)^n$ can be approximated by function $K(z) = \frac{hz}{bz^2+cz+1}$, with $c = 8\frac{n^2+4}{(n^2-4)^2}$, $b = \frac{16}{(n^2-4)^2}$, and $h = \frac{4}{n^2-4}\left(\frac{n-2}{n+2}\right)^{n/2}\left(c + \frac{8}{n^2-4}\right) = \frac{64n^2}{(n^2-4)^3}\left(\frac{n-2}{n+2}\right)^{n/2}$.

Thus, Equ. (45) becomes:

$$E\frac{\sqrt{2}z}{1+\sqrt{2}z} = \frac{hz}{bz^2+cz+1}$$

with $E = \frac{\rho\beta}{\rho^2-1}$. This is a second-degree equation in z, which, once solved in z, and due to Equ. (44), yields the abscissae of points A_{min-} and A_{min+}. This second-degree equation in z is:

$$E\sqrt{2}bz^2 + \sqrt{2}(Ec-h)z + E\sqrt{2} - h = 0$$

The condition to have real roots is: $2(Ec-h)^2 - 4E\sqrt{2}(E\sqrt{2}) - h) \geq 0$. Then, using Equ. (41), the ordinates of said points can be calculated. Those points are represented in Fig. 8 hereafter. However, it is worth mentioning that the limit condition (46) for the existence of solutions is much simpler to use.

7 Numerical simulations.

In this section, the symbolic expressions found above will be tested and illustrated. Firstly, using the approximated form of the external force, a comparison between the numerical solutions of the averaged system and the original second-order equation will test the validity of the averaging method. Secondly, using the numerical solutions of the original second-order equation, a comparison between the exact and the approximated forms of the external force will test the validity of the smoothed model versus the natural model.

7.1 Averaged system with the smoothed model of the external force: stationary condition.

Figure 8 shows a plot of the solutions of System (31), obtained by numerical calculus. The parameters are those of a typical experimental setup. Each point of the plot represents a stationary motion, i.e. a motion with constant amplitude and constant phase. The abscissae are the system's motion amplitude, while the ordinates are the excitation's, i.e. the motion amplitude of Point A represented in Fig. 1. An example of Van der Pol plot representing the solution of the averaged system (23) with the smoothed model is given in Fig. 9 for $n = 6$.

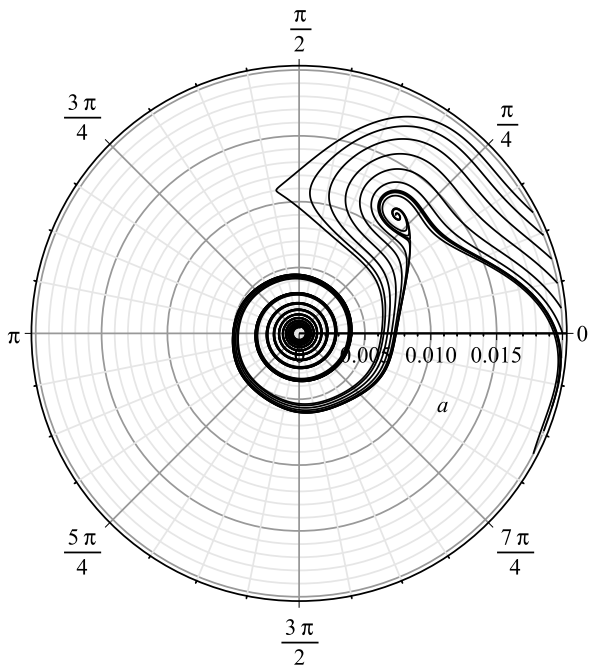

Figure 9: Van der Pol plot, averaged system with the smoothed model of the external force. a is the motion's amplitude, φ is the motion's phase. The value of a_A which is used is $7.5\ 10^{-5}$. The initial values are 0.02 for a and -0.475 for φ. The parameter values are the same as in Fig. 8.

To illustrate that the argumental phenomenon can arise for values of n greater than 4 or 6, a plot of the solution of the averaged system for the smoothed model with $n = 14$ is showed in Figs. 10 and 11.

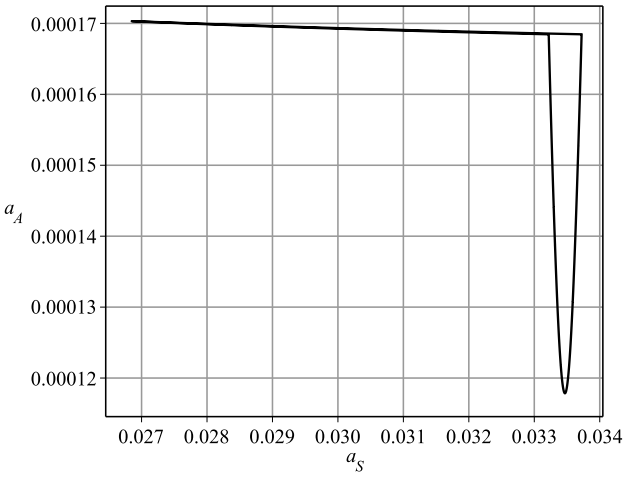

Figure 10: Stationary condition, averaged system with the smoothed model of the external force. a_S is the stationary-motion's amplitude, a_A is the excitation's amplitude. Parameter values are: $n = 14$, $\beta = 2.4\ 10^{-3}$, $F_B = 51\ N$, $F_0 = -40\ N$, $L = 0.95\ m$, $k = 250\ kN/m$, $f_{00} = 6.615\ Hz$, $f_{shaker} = 90.7578\ Hz$, $\rho_{00} = 0.98$.

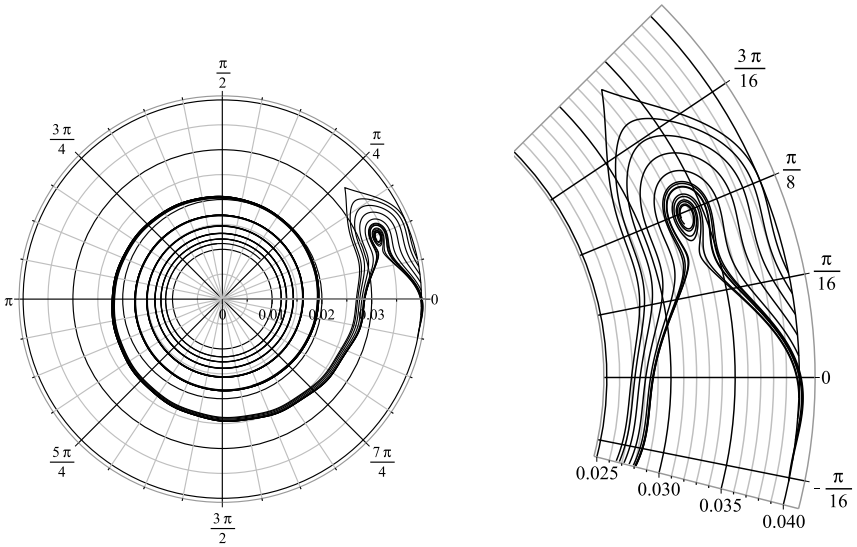

(a) (b)

Figure 11: Van der Pol representation for Fig. 10 when $a_A = 0.00015$. (a): main view, (b): zoomed view.

7.2 Original second-order equation with the smoothed model of the external force.

An example of Van der Pol plot representing the solution of the original second-order equation (23) with the smoothed model is given in Fig. 12, to be compared to Fig. 9.

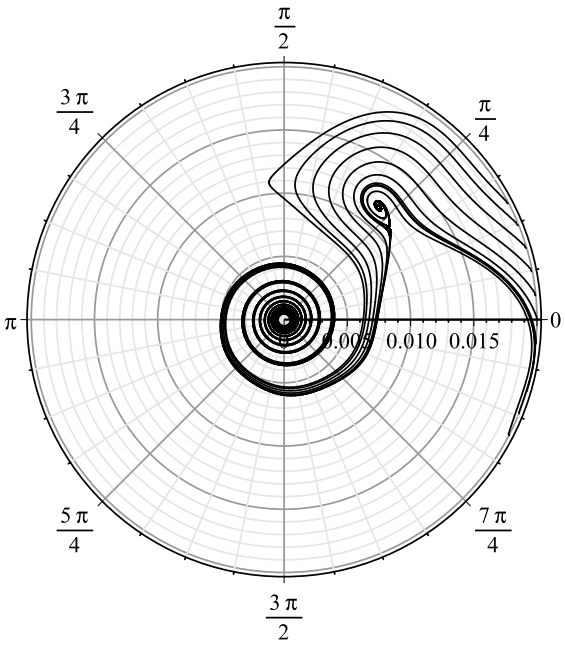

Figure 12: Van der Pol plot, original second-order equation with the smoothed model of the external force. a is the motion's amplitude, φ is the motion's phase. The parameter values and initial values are the same as in Fig. 8.

7.3 Original second-order equation with the natural model of the external force.

The solutions of the original second-order equation with the natural model (22), i.e. with the natural form of the external force, as given by Equ. (8), are obtained by the Runge-Kutta solver, giving y as a function of t. To construct the corresponding Van der Pol plots, first convert the solution into reduced-time, and then use the reciprocal relations (24), with $\rho = \nu/(\omega_0 n)$ to obtain $a(\tau)$ and $\varphi(\tau)$. Finally, smooth $a(\tau)$ and $\varphi(\tau)$. An example of Van der Pol plot obtained by this method is given in Fig. 13(a), to be compared with Figs. 9 and 12.

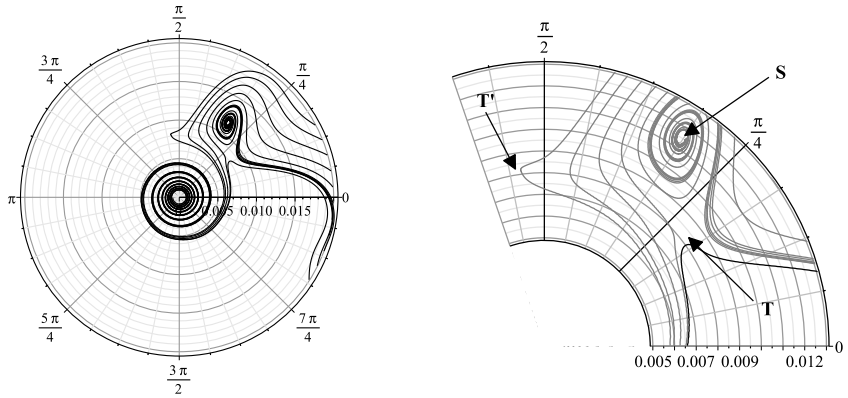

(a) (b)

Figure 13: Van der Pol plot, original second-order equation with the natural model of the external force. (a): global view; (b): detailed view. The radius is the motion's amplitude, the angle is the motion's phase. The parameter values are the same as in Fig. 8, except $a_A = 6.5\ 10^{-5}$ and initial value of $\varphi = -0.565$.

Construction of the stable and unstable stationary regime representative points relative to the natural model. Those two points are calculated in the averaged smoothed model, and denoted in this paper "S" and "T". In the natural model, they are determined graphically by observation of the Van der Pol plots. The points representing a stable stationary condition are the centers of spirals, while those corresponding to an unstable condition are the saddle type. For instance, in Fig. 13, the stable "S" point is at radius 0.0115 and angle $5\ \pi/16$, while the unstable "T" point is locatable at the peak of the curve near the point at radius 0.008 and angle $\pi/2+0.6\pi/16$, and then, knowing the problem's invariance through a rotation of $2\pi/n$, duplicated 6 times around the circle of radius 0.008, yielding a point at $\pi/2 + 0.6\pi/16 - 2\pi/6 \approx 3.26\pi/16$.

8 Discussion.

Fig. 17 shows the same data as Fig. 8, with addition of points representing the results of the natural-model simulations. The full range of values for parameter a_A yielding a stationary condition in the natural model have been explored for the parameters mentioned in Fig. 8.
Figs. 14 and 15 show a comparison between averaged system (with smoothed model) and second-order equation (with natural model) for $n = 4$. It can be seen that, for this set of parameters, the smoothed model gives results very close to those of the natural model for low values of the excitation's amplitude a_A. For high values of a_A, the smoothed model gives solutions which do not exist in the natural model. This is however on the safe side, because the assessment of hazards in civil engineering is carried out for the low values of the excitation. On the other hand, Fig. 17 shows the same comparison for $n = 6$ with a value of F_0 close to the lower limit where the argumental phenomenon disappears. It can be seen that in this case, the results of the natural model are not as close to the smoothed model as in Fig. 14, but still give a good assessment.

The comparison of the curves in Figs. 9 and 12 shows that the averaging method, for the parameters used, yields very good results. The curves in Fig. 13 are fairly close to those in Figs 9 and 12. This must be viewed in the global context of Fig. 17, where it can be seen that the parameter windows for the argumental phenomenon to arise are narrow with respect to the possible parameter ranges.
The necessity that the contact be located in a narrow parameter window explains why argumental phenomenons arise rarely in the context of structure vibration. Said windows are even narrower as n increases. The example used in Figs. 8 to 13 is for $n = 6$, but Figs. 10 and 11, to be compared with Fig. 8, show how the situation evolves when $n = 14$. In this case, the windows for a_A and a_S are respectively about 30% and 3% of the central values of a_A and a_S, against 45% and 70% for $n = 6$; the ratio F_0/F_B is 78% against 10%. Moreover, if the right amplitude excitation (a_A) is applied and the beam is given an initial amplitude larger than the corresponding a_S, the motion's amplitude will decrease due to damping, and it will then cross the crescent of Fig. 8, but only rarely be caught into the spiral, as can be seen on the Van der Pol plots. A study of the capture probability by the attractor (the spiral) is given in [6].

Figure 17 shows that the parameter ranges for the argumental oscillations to arise turn out to be quite narrow. Hence the knowledge of the symbolic formulas of the smoothed model constitute a guide to the choice of parameters for the natural model, which is closer to physical reality.

The coordinates of points representing the constant-amplitude motion, stable and unstable stationary condition, show that, given the high sensitivity of the Van der Pol representation and the zoom window used, the results of the smoothed-model simulation are indeed a good guide to those of the natural model.

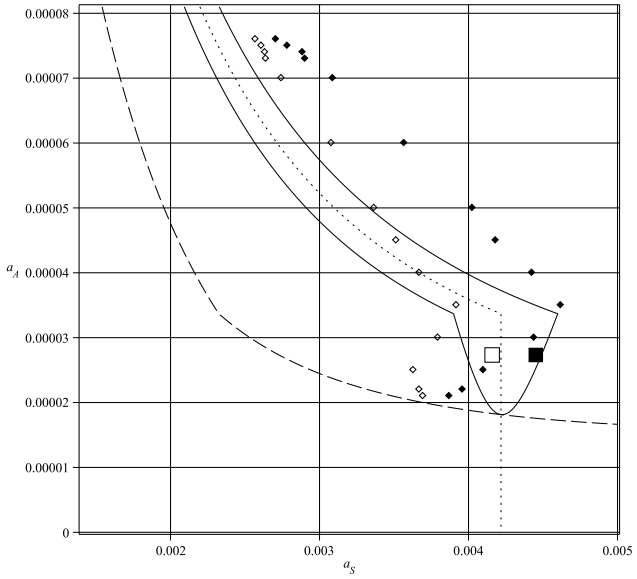

Figure 14: Stationary condition, a_A (point A's amplitude) against a_S (stationary motion's amplitude). Comparison between second-order equation (with natural model) and averaged system (with smoothed model). Parameters are: $n = 4$, $F_B = 51N$, $F_0 = -6.4N$, $f_{00} = 6.615Hz$, $\beta = 2.4\ 10^{-3}$, $L = 0.95m$, $k = 200\ 10^{-3}N/m$, $\nu = 162.419s^{-1}$. In the same way as in Fig. 8, stable (solid diamonds) and unstable (diamonds) stationary points are represented. The detailed experimental data of Fig. 31, obtained for $F_0 = -5N$, are represented as a square (unstable point) and a solid square (stable point).

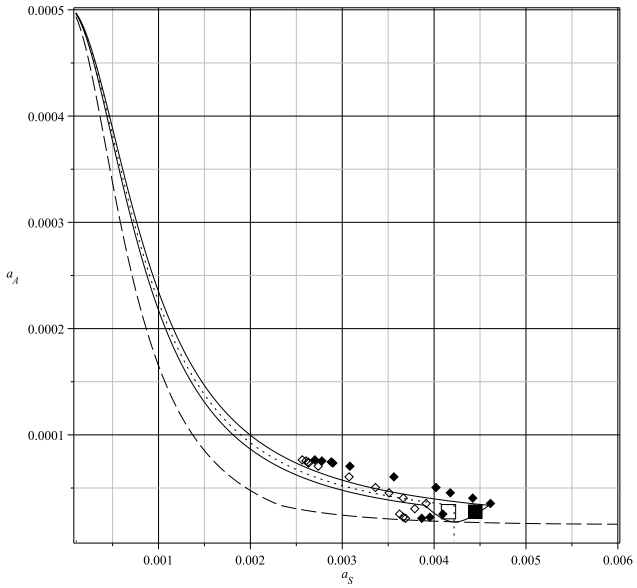

Figure 15: This view shows the whole picture containing Fig. 14.

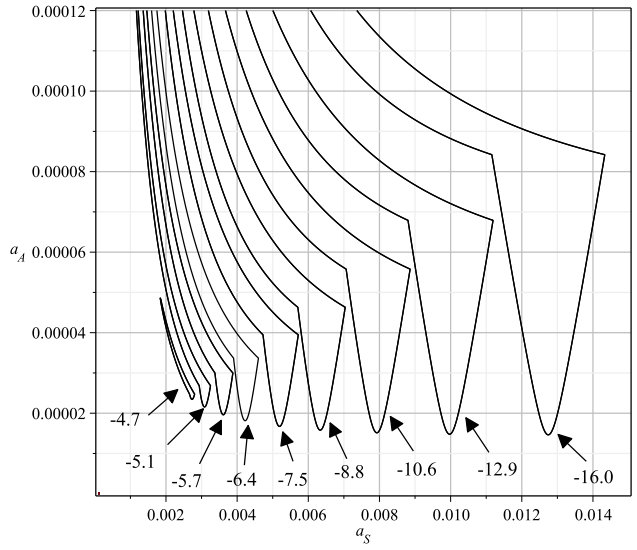

Figure 16: Stationary condition, a_A (point A's amplitude) against a_S (stationary motion's amplitude). A few curves solution for the smoothed model, for various values of F_0, denoted by arrows in the graph. Parameter values are the same as in Fig. 14.

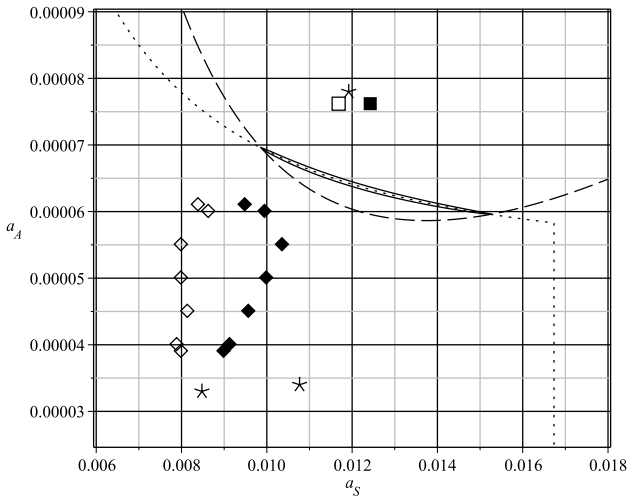

Figure 17: Stationary condition, a_A (point A's amplitude) against a_S (stationary motion's amplitude). Comparison between second-order equation (with natural model), averaged system (with smoothed model), and experiments. Parameters are the same as in Fig. 8, except $F_0 = -7.2N$. In the same way as in Fig. 8, stable and unstable stationary points are represented. The experimental detailed regime of Fig. 36, measured at $F_0 = -5N$, is represented as a solid square, while the unstable one is a simple square. Other experimental stable points maesured at $F_0 = -5N$ are represented as asterisks. Results of numerical simulations using the natural model are represented as diamonds (unstable points) and solid diamonds (stable points).

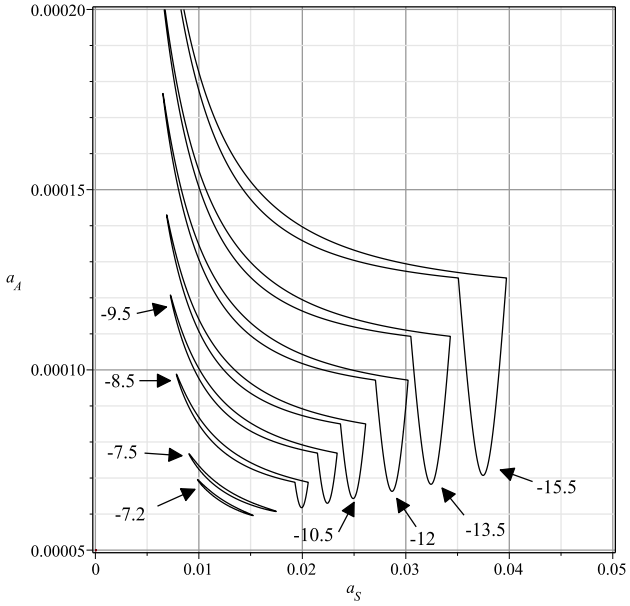

Figure 18: Stationary condition, a_A (point A's amplitude) against a_S (stationary motion's amplitude). A few curves solution for the smoothed model, for various values of F_0, denoted by arrows in the graph. Parameter values are the same as in Fig. 17.

9 Experimental setup.

In this section, the experimental setup which was used to test the cases $n = 4$ and $n = 6$ is presented, along with its calibration procedure.

9.1 Description.

To implement the arrangement shown in Fig. 1, a "beam under test" (BUT) is placed at the left-hand of the experimental setup, while the spring and point A of Fig. 1 are replaced by a second beam, called "control beam", which is excited transversally by a shaker (see Fig. 19). The point A of Fig. 1 is replaced by the junction point between the control beam and the shaker's rod, while the spring of Fig. 1 is replaced by the part of the control beam located between the shaker and the left-hand tip of the control beam. Thus, the elasticity of the spring is replaced by the flexion elasticity of said part of the control beam. Although the flexion elasticity of the control beam is not constant, the experiments and calibrations show that it can be considered constant over the displacement range of the shaker for the experiments which were carried out. Both beams are made of aluminium. The boundary conditions of the BUT are: clamped at the left end and clamped-guided at the right end, where the translational joint is achieved by means of two thin spring steel strips (0,4 mm thickness), as seen in Fig. 20, in a parallelogram configuration allowing the translation of the beam attached to them. As for the control beam, the left end is a clamped-guided joint and the right end is a decentered revolute joint. The decentered revolute joint consists of a cylinder, the circumference of which the end of the beam is attached to, and of two bearings, as illustrated in Fig. 21. Here, to minimize the rotation at the left end of the control beam, due to its small length, the distance between the strips is increased, compared to the configuration of the right end of the BUT (see Fig. 20).
In order to limit the occurrence of high-frequency modes of the BUT, its first resonance frequency is lowered by addition of local masses. Stiffeners are added to isolate the first mode by pushing aside the higher modes. The same procedure is done on the control beam. A steel ball is machined and glued on the edge of the BUT so as to provide a punctual (sphere-plane) contact between the two beams. To adjust the intermittent contact of the two beams, allowing the occurrence of the researched phenomenon, a steel spring strip (thickness of 0,1 to 0,3 mm) can be added, if necessary, between the ball and the control beam (see Fig. 20).
The measurements are carried out by two laser displacement sensors (Keyence IL-030, around $1\mu m$ resolution, time step of 0,33 ms): one near the left end of the BUT to measure its deflection (see Fig. 22), and the other one, located near the center of the control beam and in front of the shaker, to measure the deflection of the control beam. The shaker (Modalshop model 2004E), driven by a power amplifier (B&K 2719), is used to transversally excite the control beam. The connection between the shaker and the beam is made by way of a centered revolute joint (see Fig. 23).

As the position of point A of Fig. 1 must be precisely commanded, the shaker's position is controlled by a feedback loop. The global synoptic diagram is in Fig. 24. A CompactRIO controller (NI 9076) with two CompactDAQ modules (NI 9234 for the measurements acquisition and NI 9263 for the excitation signal generation) is used to carry out the active control of the shaker. Except for the feedback-control part of this diagram, the system' principle and logic implementation is the same as described in [5].

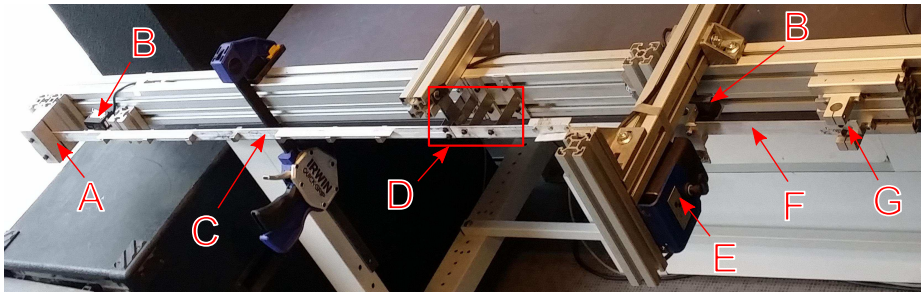

Figure 19: Experiment's global view. A: clamped joint, B: position sensor, C: beam under test (BUT), D: spring steel strips (detailed in Fig. 20), E: shaker, F: control beam, G: decentered revolute joint.

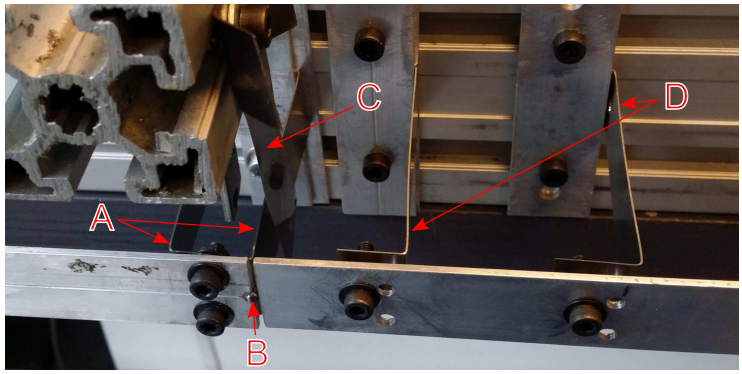

Figure 20: Contact point's environment. A: spring steel strips of the beam under test (BUT), B: steel ball at the contact point between the two beams, C: spring steel strip, D: spring steel strips of the control beam.

Remark. Although in this paper, the experiments are made with two beams so arranged that the head of the control beam has a motion frequency the same as the control beam's transverse motion, because the position at rest is offset from the rectilinear position, it can frequently happen that its head's frequency

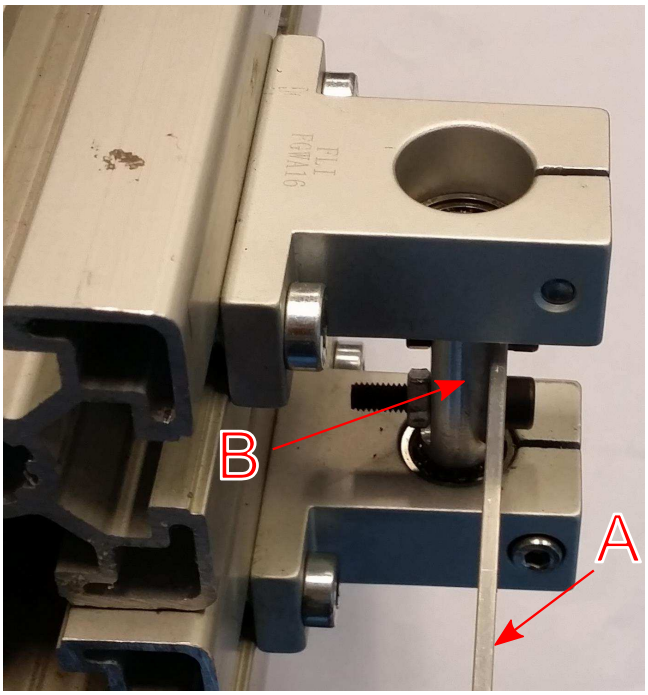

Figure 21: Control beam's pivot joint. A: control beam, B: decentered revolute joint.

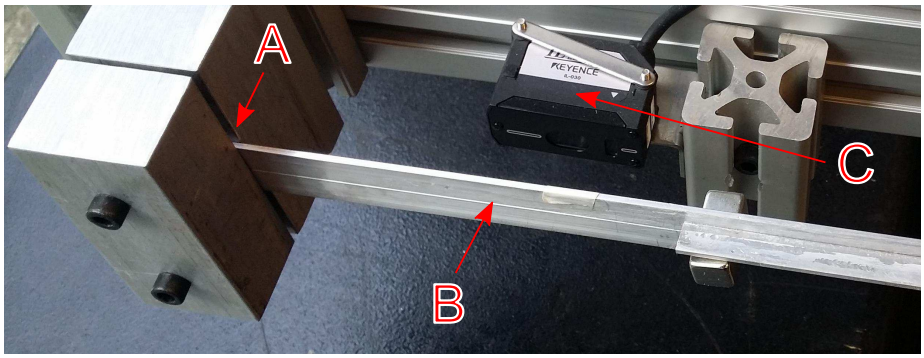

Figure 22: BUT's position measurement. A: clamped joint, B: BUT, C: position sensor.

is twice the transverse frequency. In this case, the stationary transverse frequency of the beam under test is a sub-multiple of the transverse frequency of the control beam, and the classical resonance is when both beams have the same frequency.

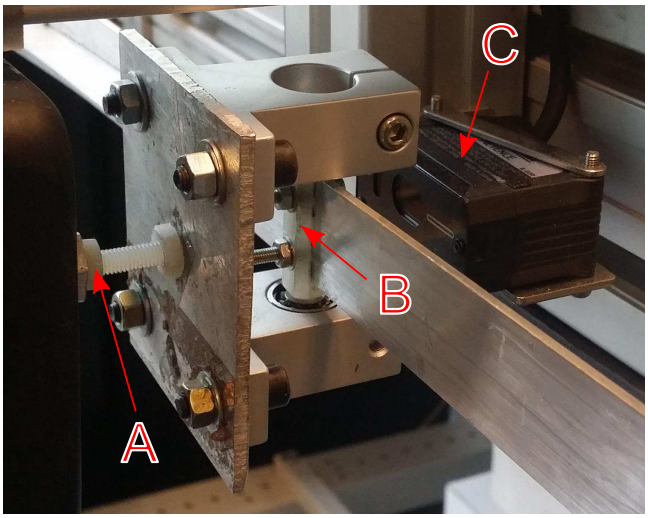

Figure 23: Shaker. A: nylon rod and nuts, B: axis of the revolute joint, C: control beam's position sensor.

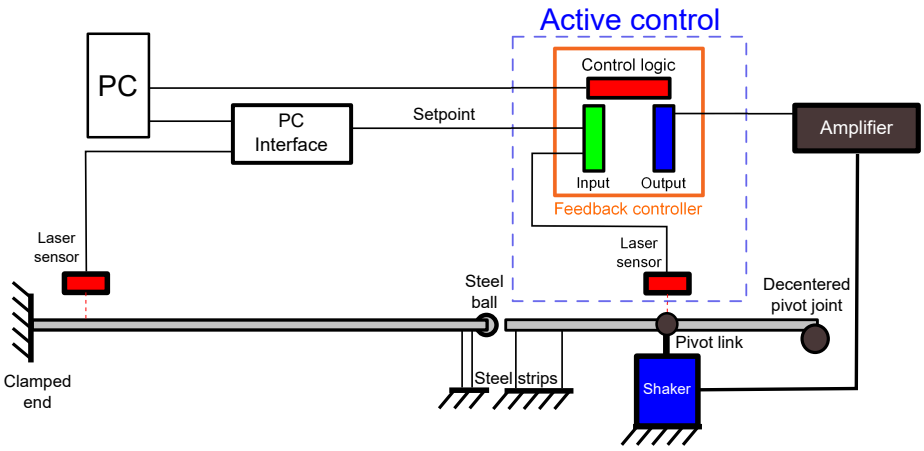

Figure 24: Global synoptic diagram.

9.2 Spectral-purity monitoring.

To ensure that the shaker does not introduce signals into the beam which induce a classical resonance of the beam, the spectral contents of the motion of point A must be monitored. As only the first mode of the beam is considered in this paper, the classical beam resonance of said first mode arises when point A's frequency is twice the beam's resonant frequency. So, measurements of the amplitudes of point A's motion and the corresponding transverse motion of the beam have been carried out at an excitation frequency of $2f_0$. Moreover, the

Table 1: Amplitude of the beam's transverse motion in response to axial excitations at f_0 and $2f_0$, for various amplitudes of point A.

Shaker's and point A's frequency	Shaker's amplitude (V pk-pk)	Point A's amplitude (mm)	Beam's amplitude (V pk-pk)	Beam's amplitude (mm/m)	Shaker's Power spectrum component
f_0	0.62	0.012	0.75	1.2	$20\ 10^{-3}$
f_0	0.38	0.0076	0.62	0.99	$8.3\ 10^{-3}$
f_0	0.19	0.0037	0.17	0.28	$1.8\ 10^{-3}$
f_0	0.024	0.00048	0.025	0.039	$1.9\ 10^{-5}$
f_0	0.012	0.00024	0.015	0.024	$1.8\ 10^{-6}$
$2\ f_0$	0.57	0.011	0.9	1.4	$5.1\ 10^{-3}$
$2\ f_0$	0.19	0.0038	0.3	0.47	$5.6\ 10^{-3}$
$2\ f_0$	0.09	0.0018	0.12	0.19	$1.3\ 10^{-3}$
$2\ f_0$	0.015	0.0003	0.04	0.063	$3.5\ 10^{-5}$
$2\ f_0$	0.005	0.0001	0.006	0.009	$3.9\ 10^{-6}$

frequency f_0 has been investigated too. The results are in Table 1. The point A's amplitude (in mm) versus the shaker's amplitude (in volts peak-to-peak) is obtained from the data in Fig. 25, which yield a slope of $0.04mm/V$. One must then divide by 2 to obtain the classical amplitude from the peak-to-peak amplitude. The beam's adimensioned amplitude (in mm/m) is obtained by multiplying the beam's amplitude (in volts peak-to-peak) by $1.5\ 10^{-3}/L$, where L is the length of the beam. The values of the shaker's spectrum components are in arbitrary unit of power.
It can be seen that if the shaker's unwanted amplitude components corresponding to the frequencies f_0 and $2\ f_0$ are kept under $3.5\ 10^{-5}$, then the corresponding unwanted beam amplitudes are kept under $0.065mm/m = 0.065\ 10^{-3}$. The hypothesis is herein made, that the order of magnitude of the beam's response due to these unwanted components at f_0 and $2\ f_0$ is still valid when these components are mixed with high-amplitude components at $4\ f_0$ or $6\ f_0$ during the experiments.

9.3 Calibration for the case $n = 4$.

Due to the very small displacements at the contact point between the BUT and the control beam, the position of the tip of the control beam has to be derived from its transverse displacement, and therefore a calibration has to be made.
First, the position of point A is measured as a function of the shaker position, given in volts by a position sensor. To do this, the resonant frequency of the beam is measured for various thicknesses of spring steel strips inserted between the two beams; by comparing the frequencies, it is possible to establish reference points and to determine, step by step, the points of Fig. 25. Then, by measuring the resonant frequency under various positions of the shaker, a relation between the position of point A and the axial force F_0 can be established. The

results are given in Fig. 26. Then, by taking the numerical derivative of F_0 with respect to x_A, the local value of the stiffness k is obtained. The results are given in Fig. 27. Finally, the value of k retained for a given experiment is obtained using a value of k in the region corresponding to the mean value of x_A of this figure. The value retained for k was $k = 200\ kN/m$.

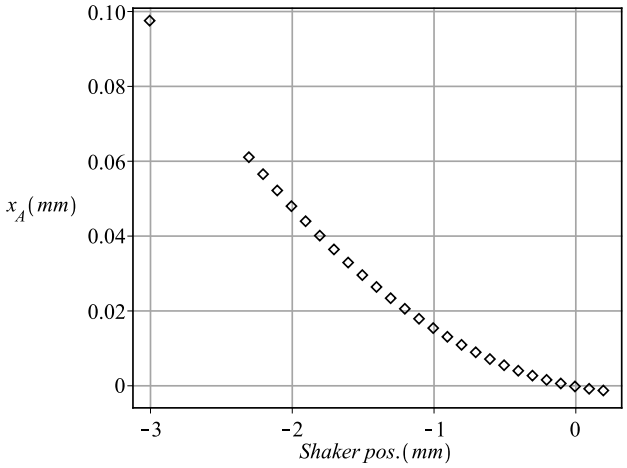

Figure 25: Point A's mean position against shaker position for the case $n = 4$. Measured points (diamonds), with the $0.1mm$ spring steel strip used in the experiments.

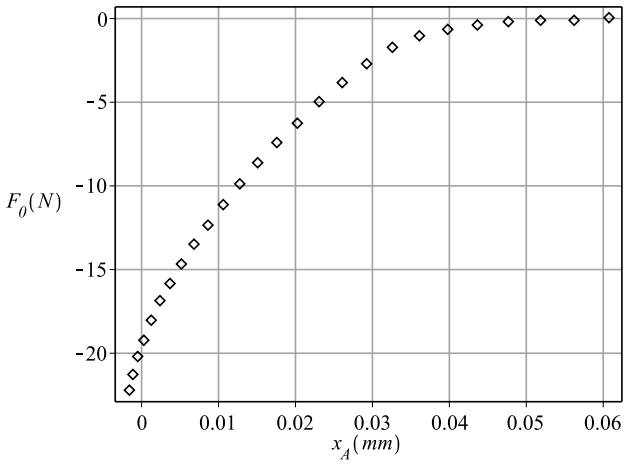

Figure 26: Axial force F_0 against point A's mean position for the case $n = 4$. Measured points (diamonds), with the $0.1mm$ spring steel strip used in the experiments.

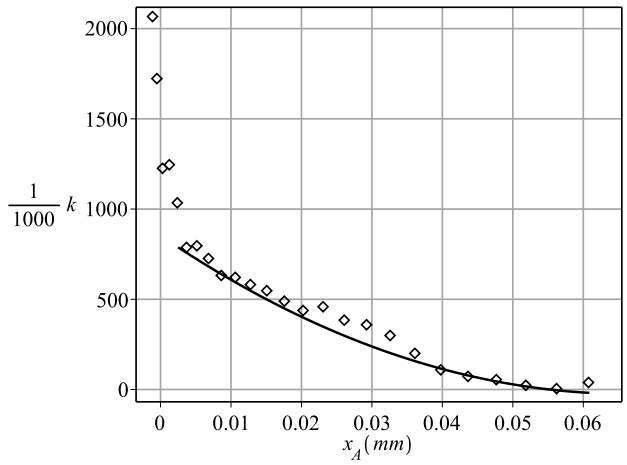

Figure 27: Stiffness k against point A's mean position for the case $n = 4$. Measured points (diamonds), with the $0.1mm$ spring steel strip used in the experiments, and trend curve in the region of interest (solid line).

9.4 Calibration for the case $n = 6$.

For the case $n = 6$, it was necessary to add a stiffener on the command beam to avoid a mode between point A and the shaker. So the value of k changed, as well as the relationship between the shaker's position and x_A. The value retained for k is now $k = 130\ kN/m$. The calibration procedure is the same as for the case $n = 4$.

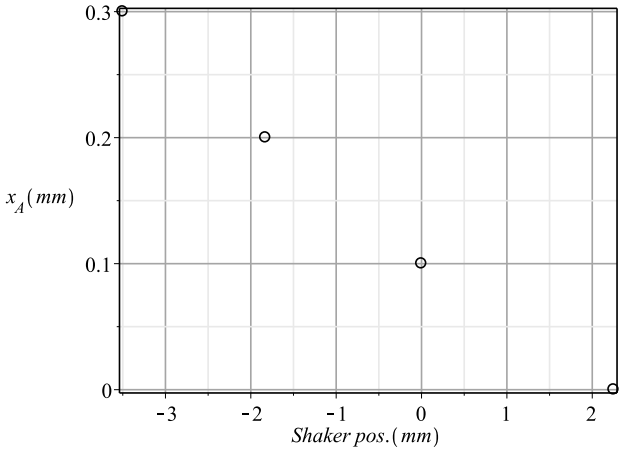

Figure 28: Point A's mean position against shaker position for the case $n = 6$. Measured points (diamonds), with the $0.1mm$ spring steel strip used in the experiments.

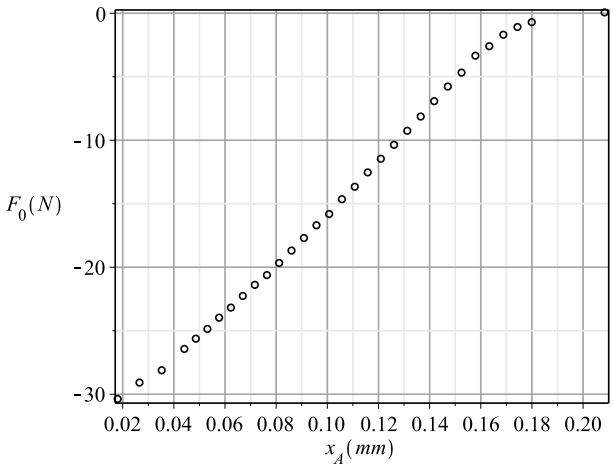

Figure 29: Axial force F_0 against point A's mean position for the case $n = 6$. Measured points (diamonds), with the $0.1mm$ spring steel strip used in the experiments.

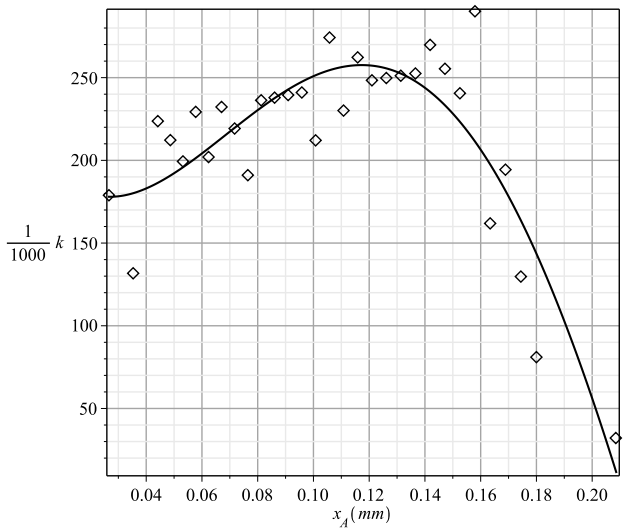

Figure 30: Stiffness k against point A's mean position for the case $n = 6$. Measured points (diamonds), with the $0.1mm$ spring steel strip used in the experiments, and trend curve (solid line).

10 Experimental results.

In this section, the experimental results are presented in Van der Pol plots, along with other detailed data about the motion and spectral purity.

10.1 Frequency ratio: $n = 4$

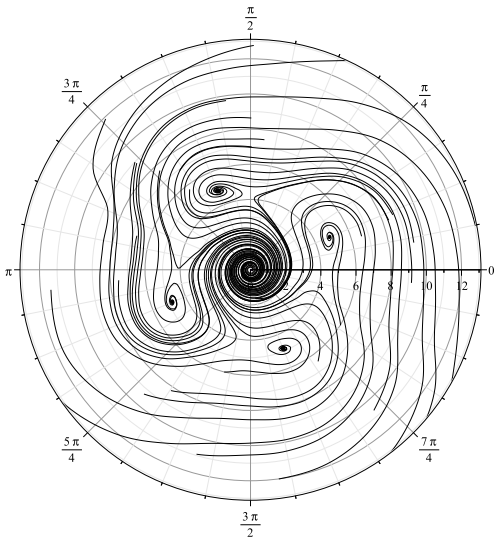

Figure 31: Experimental Van der Pol curves for n=4. The adimensioned amplitude is in mm/m. Parameters are those given about Fig. 14, except $F_0 = -5N$.

As can be seen in Fig. 33 (c) and (d), the point A's power spectrum components relative to the frequencies f_0 and 2 f_0 are kept respectively under 1.5 10^{-6} and 2 10^{-5}.

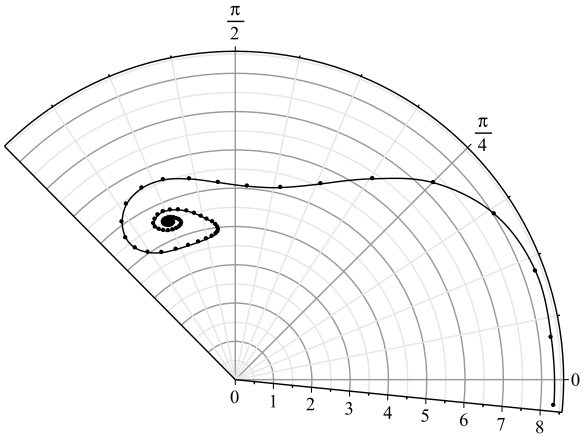

Figure 32: Detail of one curve from Fig. 31. There is one dot embedded on the curve every two periods of the beam's motion.

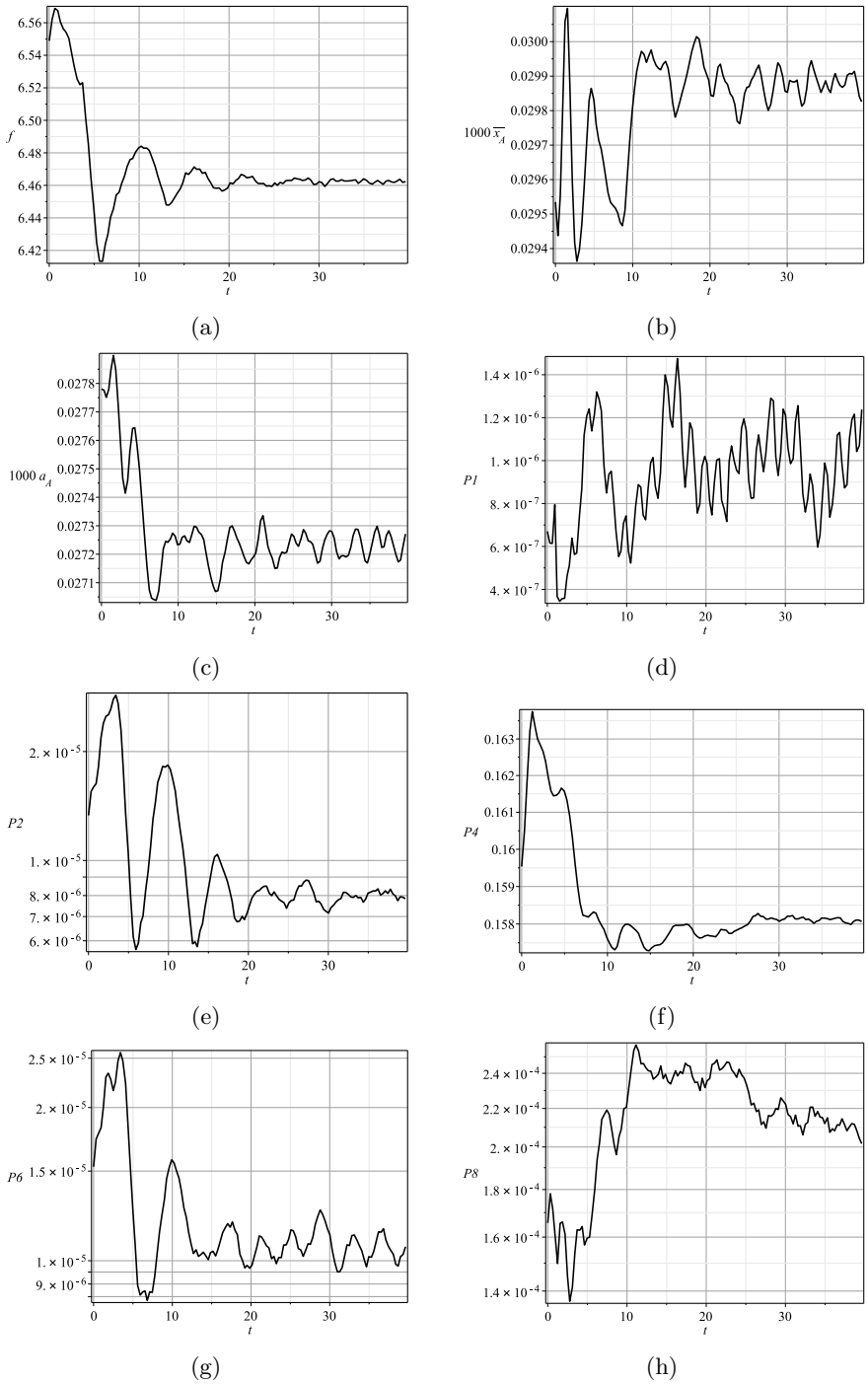

Figure 33: Details of the thread of Fig. 32: beam frequency (BF) (a), point A's mean position (b), point A's amplitude (c), and point A's spectral components at: 1 x BF (d), 2 x BF (e), 4 x BF (f), 6 x BF (g), 8 x BF (h).

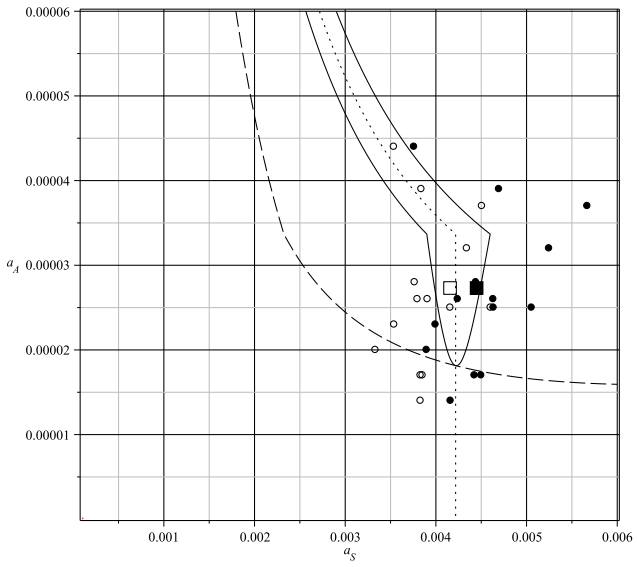

Figure 34: Stationary condition, a_A (point A's amplitude) against a_S (stationary motion's amplitude). Comparison between experimental results and averaged system (with smoothed model) for $n = 4$. Parameters are the same as for Fig. 14. Various stationary experimental points, obtained for $F_0 = -5N$, are represented: unstable points (circles) and stable points (solid circles). The detailed experimental results of Fig. 31 are represented as a square (unstable point) and a solid square (stable point).

10.2 Frequency ratio: $n = 6$

Fig. 35 shows the experimental Van der Pol curves obtained with a frequency ratio $n = 6$.
Fig. 36 shows the detail of one curve from Fig. 17. This curve lasted for $60s$.

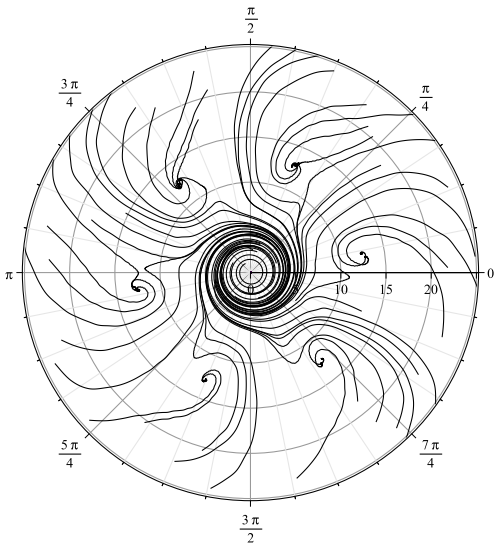

Figure 35: Experimental Van der Pol curves for n=6. The adimensioned amplitude is in mm/m. Parameters are those given about Fig. 17, except $F_0 = -5N$.

As can be seen in Fig. 37 (c) and (d), the shaker's components relative to the frequencies f_0 and 2 f_0 are kept respectively under 3.5 10^{-5} and 1.6 10^{-5}.

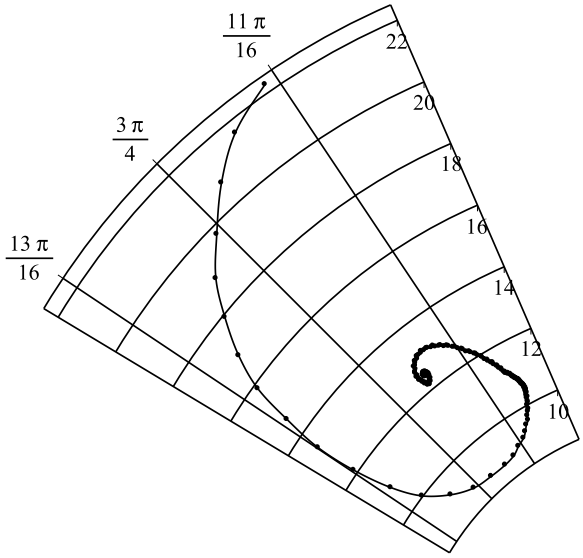

Figure 36: Detail of one curve from Fig. 35. There is one dot embedded on the curve every two periods of the beam's motion.

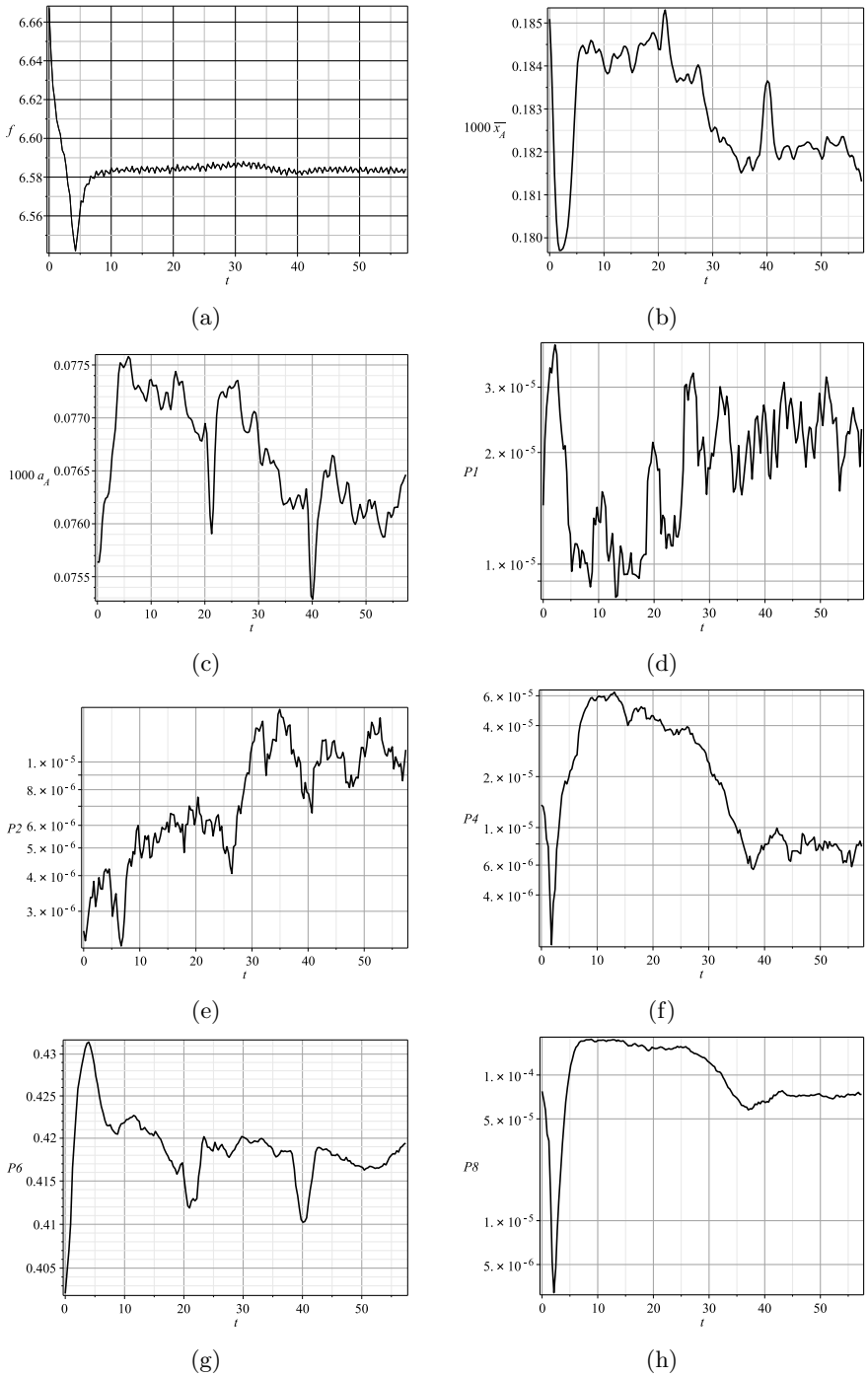

Figure 37: Details of the thread of Fig. 36: beam frequency (BF) (a), point A's mean position (b), point A's amplitude (c), and point A's spectral components at: 1 x BF (d), 2 x BF (e), 4 x BF (f), 6 x BF (g), 8 x BF (h).

11 Conclusion.

It has been shown that when a beam under test is submitted to an harmonic axial excitation through a permanent or an intermittent elastic contact, it can enter a stationary regime where its transverse vibration has a frequency which is a sub-multiple of half the frequency of the axial excitation. Besides the classical resonant case, where the axial excitation is twice the fundamental frequency of the beam, this constitutes an argumental phenomenon.
This situation can be encountered when two beams are placed head-to-head, in axial contact.

12 Appendix A.

In this Appendix, the tangential condition between the curves representing function $y_1(z) = E\left(1 - \frac{1}{z} + \frac{1}{z\sqrt{2z+1}}\right)$, and function $y_2(z) = \frac{1}{z}\left(\frac{\sqrt{1+z}-1}{\sqrt{z}}\right)^n$ will be studied for z real positive, $n \geq 4$, and E =positive constant.

12.1 Function $y_1(z) = E\left(1 - \frac{1}{z} + \frac{1}{z\sqrt{2z+1}}\right)$.

This function is an increasing function for $z > 0$. Near zero, the function is equivalent to $3\,z/2 - 5\,z^2/2$. The asymptotic limit for $z \to +\infty$ is 1. The plot for $E = 1$ is in Fig. 38.

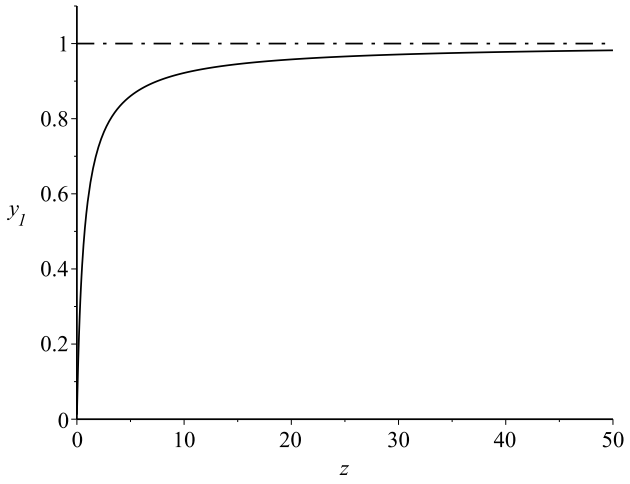

Figure 38: Plot of $y_1(z)$, with $E = 1$.

12.2 Function $y_2(z) = \frac{1}{z}\left(\frac{\sqrt{1+z}-1}{\sqrt{z}}\right)^n$.

This function is defined for every real positive z, and can be extended to 0 in $z = 0$.

Near zero, the function is equivalent to $\frac{z^{\frac{n}{2}-1}}{2^n}$.

Near infinity, the function is equivalent to $\frac{1}{x}\left(1 - \frac{n}{\sqrt{z}}\right)$.

The function increases from $z = 0$ to $z_{2max} = \frac{n^2}{4} - 1$, then decreases asymptotically to 0.

The value of the maximum is $y_{2max} = \dfrac{4}{n^2-4}\left(\dfrac{n-2}{n+2}\right)^{n/2}$.
The plot for $n = 6$ is in Fig. 39.

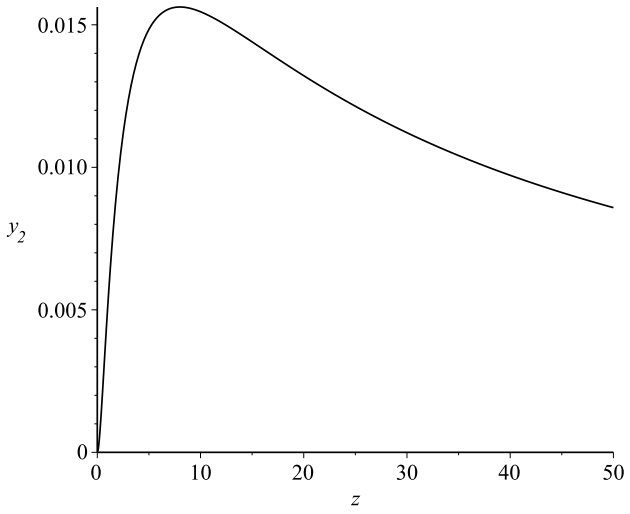

Figure 39: Plot of $y_2(z)$, with $n = 6$.

12.3 Tangency of functions $y_1(z)$ and $y_2(z)$.

Knowing the behaviour of functions y_1 and y_2, one is led to consider that both curves are tangent approximately at the maximum of y_2, provided that $y_1(z_{2max}) = y_{2max}$. Hence the value E_{tan} of E which satisfies this tangency must verify:

$$E_{tan}\left(1 - \frac{1}{z_{2max}} + \frac{1}{z_{2max}\sqrt{2z_{2max}+1}}\right) = \frac{4}{n^2-4}\left(\frac{n-2}{n+2}\right)^{n/2}$$

Taking the approximation

$$1 - \frac{1}{z_{2max}} + \frac{1}{z_{2max}\sqrt{2z_{2max}+1}} \approx 1 - \frac{4}{n^2} \tag{48}$$

for $n \geq 4$, one finally gets:

$$E_{tan} \approx \frac{4n^2}{(n^2-4)^2}\left(\frac{n-2}{n+2}\right)^{n/2} \tag{49}$$

As for the tangency point's ordinate, assume that it is the same as the maximum of the $y_2(z)$ curve, i.e. y_{2max}. Note that $E_{tan} = \dfrac{n^2}{n^2-4}\, y_{2max}$.
The following hypothesis is made:

- For $E < E_{tan}$, the curves of y_1 and y_2 intersect in $z = 0$ and at least in two other points, one located at $z < z_{2max}$ and one at $z > z_{2max}$.

- For $E > E_{tan}$, the curves of y_1 and y_2 intersect in $z = 0$.

A typical case is represented in Fig. 40 for $n = 6$ and $E_{tan} = 9/512$ according to Equ. (49). On the plots, it can be seen that the value of y_1 in z_{2max} is slightly greater than expected. This is due to approximation (48), which partially compensates for a better tangency estimate. Other values of n give similarly good results for E_{tan}, except for $n = 4$, where it is better to use a value of $1.03\, E_{tan}$.

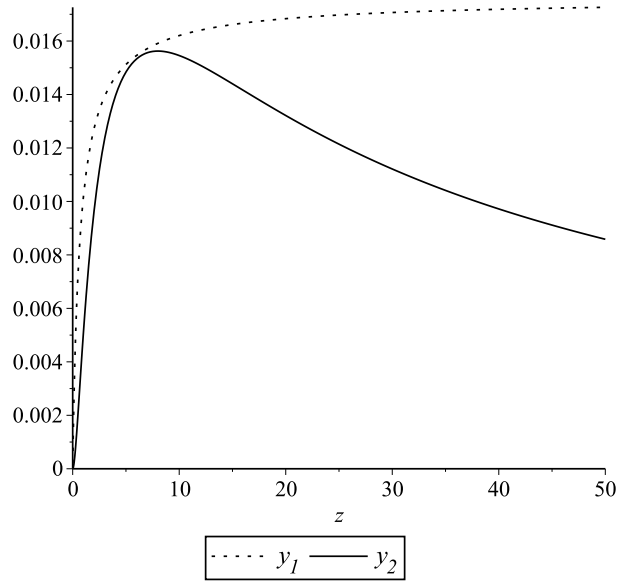

Figure 40: Tangency of $y_1(z)$ and $y_2(z)$, with $n = 6$.

References

[1] M.J. Béthenod. Sur l'entretien du mouvement d'un pendule au moyen d'un courant alternatif de fréquence élevée par rapport à sa fréquence propre. *Comptes rendus hebdomadaires de l'Académie des sciences*, 207(19):847–849, November 1938. (in French).

[2] N. Bogolioubov and I. Mitropolski. *Les méthodes asymptotiques en théorie des oscillations non linaires*. Gauthiers-Villars, 1962.

[3] D. Cintra. *Le phénomène d'oscillations argumentaires et son application au génie civil*. Ph. d. thesis, Ecole des Ponts ParisTech, 2017.

[4] D. Cintra and P. Argoul. Non-linear argumental oscillators: Stability criterion and approximate implicit analytic solution. *Journal to be determined*, 2016. (submitted).

[5] D. Cintra and P. Argoul. Nonlinear argumental oscillators: A few examples of modulation via spatial position. *Journal of Vibration and Control*, 2016. (online publication, pre-printing).

[6] D. Cintra and P. Argoul. Attractor's capture probability in nonlinear argumental oscillators. *Communications in Nonlinear Science and Numerical Simulation*, 48:150 – 169, 2017.

[7] B. Cretin and D. Vernier. Quantized amplitudes in a nonlinear resonant electrical circuit. In *2009 Joint Meeting of the European Frequency and Time Forum and the IEEE International Frequency Control Symposium, vols 1 and 2*, volume 1 & 2, pages 797–800, Besançon, France, April 2009. Joint Meeting of the 23rd European Frequency and Time Forum/IEEE International Frequency Control Symposium.

[8] D. Doubochinski. *Argumental oscillations. Macroscopic quantum effects.* SciTech Library, August 2015.

[9] D.B. Doubochinski and J.B. Doubochinski. Amorçage argumentaire d'oscillations entretenues avec une série discrète d'amplitudes stables. *E.D.F. Bulletin de la direction des études et recherches, série C mathématiques, informatique*, 3:11–20, 1991. (in French).

[10] X. Nayfeh. Transverse... *Journal X*, 67:8, June-July 1965.

[11] D. I. Penner, D. B. Doubochinski, M. I. Kozakov, A. S. Vermel, and Yu. V. Galkin. Asynchronous excitation of undamped oscillations. *Soviet Physics Uspekhi*, 16(1):158–160, July-August 1973.

[12] J.P. Treilhou, J. Coutelier, J.J. Thocaven, and C. Jacquez. Payload motions detected by balloon-borne fluxgate-type magnetometers. *Advances in Space Research*, 26(9):1423–1426, 2000.